THE RINGS OF URANUS

J. L. ELLIOT
Massachusetts Institute of Technology

and

P. D. NICHOLSON
Cornell University

Uranus is encircled by nine narrow rings, denoted 6, 5, 4, α, β, η, γ, δ and ε, in order of increasing distance from the planet. The rings have been observed at high spatial resolution (3.5 km) during 13 stellar occultations from 1977 to 1983. Sharp edges are characteristic of the ring structures, whose optical depths range from ~0.5 to values of ~1.5 and greater. The widths of most rings lie between 2 and 12 km, with two exceptions. The η Ring has a narrow core a few km wide adjacent to a broad component ($\tau \sim 0.1$) ~55 km wide. The width of the ε Ring varies, as a linear function of its radius, from 20 km at periapse to 96 km at apoapse. The widths of the α and β Rings also vary approximately linearly with their radii. A Keplerian model, including five orbital elements for each ring, has been successfully fitted to the occultation data. The semimajor axes are found to lie between 41877 km (Ring 6) and 51188 km (ε Ring). The largest eccentricity is 7.94×10^{-3} (ε Ring), while the γ and η Rings cannot be distinguished from circles ($e < 10^{-4}$). Seven of the nine rings are inclined to the planet's equatorial plane by a few hundredths of a degree. The orbit solution yields values for the Uranian gravitational harmonic coefficients $J_2 = (3.349 \pm 0.005) \times 10^{-3}$ and $J_4 = (-3.8 \pm 0.9) \times 10^{-5}$, which can be used to constrain interior models of Uranus. Infrared imaging observations confirm the derived precession rate for the ε Ring and place limits on the optical depth of inter-ring material. Spectra of the rings show their geometric albedo to lie between 0.02 and 0.03 in the wavelength range 0.89–3.9 μm, ruling out ice-covered particles. Several lines of evidence suggest that the "average" ring particles are larger than 1 μm. The main theoretical problems still posed by the Uranian rings concern their sharp edges and the internal structures exhibited by the α, η and ε Rings. New information about the rings will be provided by further groundbased observations, the Space Telescope and the Voyager encounter in January 1986.

In this chapter we survey current knowledge concerning the Uranian rings, and explain how this knowledge has been derived from the observations. For each ring system we have the ultimate goal of learning its origin and its evolution to its present state, as described by (i) the composition of the ring particles, (ii) the distribution function of particle sizes, and (iii) the dynamical processes that determine the particle orbits. Although we are far from this goal for the Uranian system, we do know a great deal, particularly about its kinematics. In fact, the discovery of the Uranian rings in 1977 marked the beginning of the current renaissance in studies of planetary rings, and the Uranian system has made some notable contributions to our studies of all ring systems. The phenomena first observed in the Uranian system are:

1. Narrow rings (inspiring confining satellite models);
2. Sharp edges;
3. Long-lived structure in the radial direction on kilometer scales (ϵ Ring);
4. Eccentric rings;
5. Inclined rings;
6. Uniform apsidal and nodal precession;
7. Adjacent broad and narrow ring components (η Ring);
8. Low albedo ring particles.

Most of the items in the above list were discovered through the high spatial resolution provided by stellar occultations, presently the principal method used to observed the Uranian rings. Observation of a stellar occultation provides a trace of the transmitted starlight as a function of position in the ring system. For groundbased observations of occultations at near-infrared wavelengths, the limit to the *spatial resolution* is ~ 3.5 km for the structural features in the rings and about 0.1 km in the *position* of a sharp feature, such as an edge. The 3.5-km resolution compares to a resolution of $\sim$ 10,000 km achievable with groundbased imaging and is somewhat better than the resolution achieved by Voyager imaging and radio occultation observations of Saturn's rings. It is about one and a half orders of magnitude worse than the resolution of 0.1 km achieved by the Voyager photopolarimeter occultation observations at Saturn.

With these high-resolution occultation data, we have been able to construct a good kinematic model for the ring orbits and have begun to characterize the structure of individual rings. The picture that emerges from these studies (see Fig. 1) is of a system of nine, sharp-edged rings; they are relatively opaque, narrow ($\lesssim$2 to 100 km) and separated by broad (300–2500 km) gaps. Reports of other material have been made, but not confirmed. Current upper limits on the optical depth of inter-ring material are ~ 0.05, based on occultation data, and ~ 0.003, based on images of the rings at 2.2 μm (see Sec. IV). At least six of the rings are measurably eccentric (i.e., $e \gtrsim 10^{-4}$), a

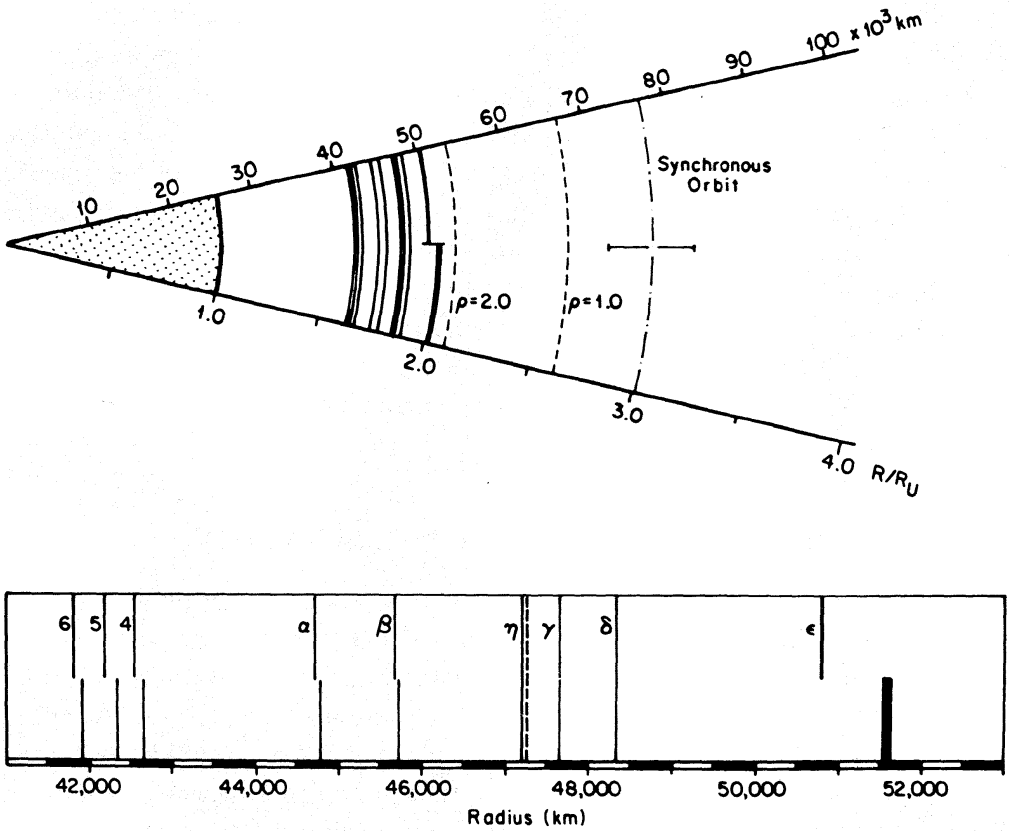

Fig. 1. Schematic diagram showing the locations of the nine confirmed rings of Uranus. The dashed arcs represent the Roche limits for satellite densities of 1.0 and 2.0 g cm^{-3}, while the dot-dashed arc corresponds to the synchronous orbit distance for a planetary rotation period of 15.6 ± 1.4 hr (see Sec. V). The lower portion of the diagram shows the radial region which spans the known rings, enlarged by a factor of 10. For each of the 6 definitely eccentric rings (see Sec. III) both the minimum (periapse) and maximum (apoapse) radii are indicated. The width of the ϵ Ring, which varies markedly from periapse to apoapse, is plotted to scale; the other rings all have widths of <10 km, below the resolution of this figure. The outer boundary of the η Ring's broad component (Sec. II) is indicated by a dashed line.

characteristic shared by several narrow ringlets in the Saturnian system (see chapter by Cuzzi et al.). Perhaps even more surprising is the fact that the nine rings do not lie exactly in the same plane. Their inclinations relative to Uranus' equatorial plane are of the same order as the eccentricities (with one notable exception), but are more difficult to measure because of the currently almost pole-on aspect of the planet.

The outermost ring, designated ϵ, is broad enough to reveal long-lived internal structure. The α Ring sometimes shows a "double-dip" in transmitted light during stellar occultation, perhaps indicating an internal division, and the η Ring has a broad component of low optical depth. The widths of the inner trio of rings, designated 6, 5, and 4, are below the diffraction limit of Earth-based observations (~ 3.5 km at a wavelength of 2.2 μm).

Near-infrared observations of the ring system indicate that the ring particles have extremely low geometric albedos (0.02–0.03) and an essentially flat 1–4 μm spectrum. Apart from their intrinsic interest, the rings serve both as an ensemble of test particles for studies of Uranus' gravitational field and as a precise reference system for studies of the shape and orientation of the planet.

Before proceeding to a detailed description of the structure and kinematics of the rings in Secs. II and III, we review briefly the techniques and limitations of groundbased stellar occultation studies of ring systems in general, and of the Uranian system in particular. Previous reviews of the Uranian ring system, from observational and theoretical viewpoints, have been given by Brahic (1982), Elliot (1982), and Goldreich and Tremaine (1982).

I. STELLAR OCCULTATION OBSERVATIONS

The essential features of a stellar occultation observation are simply described as follows. The occulting body (planet, satellite, or ring) casts a shadow in the light from the star, through which the Earth passes in its orbital motion. Since the distance of the star is effectively infinite, the shadow at the Earth is a full-scale, two-dimensional projection of the occulting body. In the case of the Uranian rings, the maximum dimension of the shadow is $\sim$8 times the diameter of the Earth and only a limited portion of the system can be studied during any one occultation. Typically, the projected velocity of the Earth across the shadow is 10–30 km s^{-1}, although lower velocities are possible for occultations that occur near the "stationary" points in the planet's geocentric motion.

When a stellar occultation is observed, the intensity of starlight is recorded as a function of time as the Earth moves relative to the occulting body. In other words, the intensity of starlight is measured along a single line through the two-dimensional shadow pattern. This situation is illustrated schematically in Fig. 2, for a central occultation by a ringed planet. Note that, while the extinction of starlight by a ring can be related to the optical depth (and width) of the ring, the decrease in intensity as the starlight penetrates the planet's atmosphere is due to differential refraction, rather than to absorption (see the review by Elliot [1979]).

The fundamental limit on the resolution achievable from a stellar occultation is set by diffraction. At typical Uranus-Earth distances, $D \sim 18$ AU, and at the usual observational wavelength, $\lambda = 2.2$ μm, this limit is $\sim(2\lambda D)^{\frac{1}{2}} =$ 3.5 km, as measured by the full width at half maximum (FWHM) of an occultation profile for a narrow ring.

A. Occultation Predictions

The first step in an observational program for occultations is to obtain predictions for those occultations whose signal-to-noise ratio would be suffi-

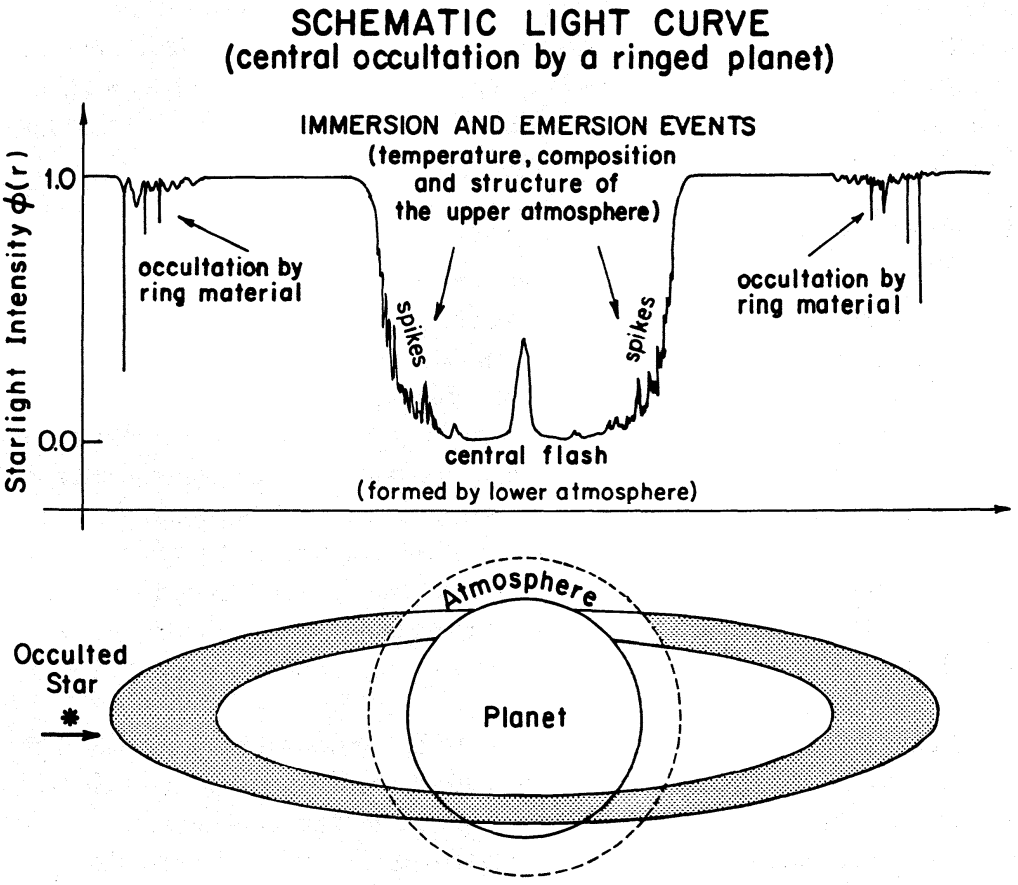

Fig. 2. Schematic lightcurve for a central occultation by a ringed planet. The upper portion of the figure shows the light intensity of the star that would be observed from Earth as a function of the position of the star behind the planet. The first attenuation of starlight is due to the extinction by the ring material. The occultation of the star by the atmosphere occurs through the process of differential refraction, with irregular variations (spikes) caused by atmospheric structure that deviates from being isothermal. The central flash is observed when the star is directly behind the center of the planet and can yield information about the extinction of the lower atmosphere (figure after Elliot 1979).

cient to produce useful information about the rings. One method to predict occultations is to compare the ephemeris of Uranus with stellar positions in the Smithsonian Astrophysical Observatory (SAO) catalog. This technique was used by Taylor (1973) to predict the occultation of SAO 158687 by Uranus on 10 March 1977, during which the rings were accidentally discovered (Elliot et al. 1977*a*; Elliot 1979). However, occultations of SAO catalog stars by Uranus are rare. Furthermore, the SAO catalog does not contain most of the stars whose occultations are observable at 2.2 μm. To identify additional events, one must obtain plates of the star fields ahead of Uranus, measure the positions of stars in Uranus' path, and then calculate the circumstances for the occultations observable from Earth. From these candi-

dates, only the sufficiently bright stars are selected for the final list of events, which occur at a rate of about two per year. This method of predicting and evaluating occultations for the Uranian rings was developed by Klemola and Marsden (1977), Liller (1977) and Elliot (1977). A list of predictions through 1984 has been published by Klemola et al. (1981).

B. Observational Techniques

The goal of occultation photometry is to measure the intensity of the starlight as a function of time; these data are then readily converted to optical depth as a function of radius for the individual rings. Observations of the same occultation from different sites are valuable because they correspond to different tracks through the ring system and give information about the two-dimensional structure of the ring occultation pattern. Simultaneous observations at different wavelengths, from the same site, give information about the distribution of the ring particle sizes and allow discrimination against some forms of noise in the photometry discussed below. Primary concerns in carrying out the observation are (i) to obtain photometry with the greatest possible signal-to-noise ratio, and (ii) to be sure that the data are accurately synchronized with Universal Time (UT).

Let us now consider the factors involved in obtaining photometry of high signal-to-noise ratio. Since the rings are at most only 2 arcsec from the limb of Uranus, at least some, if not all, of the light from Uranus is included within the photometer aperture along with the starlight. For our purposes, the light from Uranus constitutes a background and is a source of noise. One method of minimizing this contribution is to observe in one of the methane bands, which become progressively deeper in the spectrum of Uranus at longer wavelengths (Fink and Larson 1979). Within wavelengths accessible to photomultipliers, the methane band at 8900Å is the deepest (Elliot et al. 1977*c*). In the near infrared, the 2.2. μm band is so deep that Uranus is even fainter than the rings themselves. This band nicely matches the passband of the K filter, which has become standard for observing ring occultations.

For the data obtained to date, a variety of noise sources have proven to be important. For each particular occultation, the significant noise sources depend on the prevailing conditions and observing set-up. The sources of noise that occur are the following:

1. Photon (shot) noise from both Uranus and the occulted star;
2. Scintillation noise from both planet and star;
3. Light from both planet and star spilling out of the photometer aperture due to time variations in the seeing;
4. Changes in transparency of the atmosphere due to clouds;
5. Uncompensated sky background variations (for infrared observations);
6. Variations in signal due to telescope guiding errors (if the beam profile of the photometer is not flat);

7. A host of infrequent, sometimes not understood, "glitches" which are probably due to momentary problems with the signal processing electronics or isolated, small clouds that are not otherwise noticed by the observer.

To obtain useful data for the analyses that will be discussed later in this chapter, the observer should perform several calibrations. Well before the event, the signals from both Uranus and the occulted star should be measured through the available filters in order to determine which would give the best signal-to-noise ratio (Elliot 1977). At this time it would also be wise to check the beam profile of the photometer and do whatever possible to make it flat. The timing system should be carefully traced and well understood. Timing based on hardware is usually better than software, since additional timing uncertainty is introduced by the computer-interrupt system. Just before the observations, these earlier calibrations should be verified and the size of the photometer aperture selected to be compatible with the seeing conditions. The aperture should not be so small that light spilling out during moments of the worst seeing is a source of noise. The step response of the entire system should be well measured. Also, it has proven prudent to carefully monitor the signal continuously, with a chart recorder, and to note any known causes for events seen in the signal as they occur. Frequent calibration of the background and star signal levels is desirable.

Synchronizing the observation with UT is accomplished through radio time signals. The accuracy achievable with this method is limited by the uncertainty in the propagation delay of the radio signals, which should be $\leqslant$ 0.01 s. The timing synchronization should be confirmed both immediately before and after the data recording for the event.

C. Limits to Spatial Resolution

The limiting spatial resolution for a given occultation depends on four main factors:

1. Diffraction;
2. Angular diameter of the star;
3. Signal-to-noise ratio of the data;
4. Impulse response of the observing equipment.

The effects of each of these factors can be best explained by tracing the path of the starlight through the rings, and into the telescope. Then we consider how the starlight is detected and how the resulting signal is processed and recorded. A plane wave from a distant point source encounters the rings, and the light not scattered or absorbed by the ring particles emerges on the other side of the rings and continues on its path through space. To learn its intensity pattern at a given distance from the rings, we must calculate the

diffracted intensity for this distance. Complicated diffraction effects can arise, but for our present purpose, we can simply note that the spatial resolution is degraded by $(2\lambda D)^{\frac{1}{2}}$ where λ is the wavelength of the light and D is the distance from the rings to the observer. As discussed earlier in this section, this limiting resolution for $\lambda = 2.2$ μm is ~ 3.5 km in the sky plane, for typical distances between the Earth and Uranus. We can think of this limit as a circular "beam profile" in the sky plane, which is a plane passing through the center of Uranus, perpendicular to the line of sight. Projected into the plane of a ring, this beam profile becomes an ellipse that has a minor axis equal to the diameter of the circular beam profile in the sky plane. Along the minor axis of the ellipse, the resolution in the ring plane is the same as in the sky plane. However, the resolution is degraded by a factor csc B along the major axis of the ellipse, where B is the angle between the line of sight and the ring plane.

Presently, B is about 70° for the Uranian rings, so that the resolution limit in the ring plane essentially equals that in the sky plane. When B becomes significantly smaller, the csc B factor becomes appreciably > 1, as is always the case for Saturn. However, its effect on degrading the radial resolution in the ring plane depends on the orientation of the elliptical beam profile relative to the path of the star through the ring system. For example, if the occultation track were along the line joining the ansae of the rings, the *radial* resolution would not be degraded from the sky plane diffraction limit. However, the beam would be expanded in the *azimuthal* direction by the csc B factor.

Since the star has a finite angular diameter, the point-source diffraction pattern of a ring is convolved with the intensity distribution function across the stellar disk. For a bright star of later spectral type, the resulting degradation of spatial resolution can dominate diffraction. The relevant parameter is the length subtended by the angular diameter of the star over the distance between Uranus and the Earth (see Table I).

Relativistic bending of the starlight by the planet's gravitational field results in a nonuniform radial shrinkage of the shadow, but does not affect the spatial resolution. For light grazing the limb of Uranus, this shrinkage amounts to ~ 25 km at the distance of Earth.

Intrinsic to this light is the photon noise and whatever modulation is added on its path through the Earth's atmosphere. The critical parameter is the noise within the time that the star moves an element of spatial resolution in the ring plane, say, the diffraction limit. Hence, the noise in the time domain is scaled by the relative velocity (projected into the ring plane) of the Earth and Uranus. This velocity is typically 20 km s^{-1}, but can vary from a few to ~ 30 km s^{-1}.

After the light arrives at the telescope, it is detected and recorded. For observations at visible wavelengths, the detector is a photomultiplier, which has a negligibly short response time. The number of detected photons can be integrated over a short time and then recorded, with a negligible dead time between integrations. For infrared observations with star-sky chopping, the

process is more complicated. For these data, we have a detector time constant to contend with, and the beam is chopped between star and sky so that the star is observed only half of the time. The chopped signal is filtered, integrated and recorded. All of these processes can add significant response time to the data. The combined effect of these processes can be determined through measuring the step response of the system. One method for doing this is to rapidly move a star out of the center of the photometer aperture, if the telescope can be accelerated quickly enough.

D. Summary of Observations

All known occultation observations of the Uranian rings, through the 1983 apparition, are summarized in Table I. The star designations KM and KME refer to the lists of occultation candidates published by Klemola and Marsden (1977) and Klemola et al. (1981). For each star, the V (0.56 μm) and K (2.2 μm) magnitudes are given, together with its estimated angular diameter. In the last two columns, the number of sites at which observations were obtained and references to published data are given. A typical set of recordings, showing all nine rings, is presented at low spatial resolution in Fig. 3.

Reports of possible other material in the ring system have been made by Millis and Wasserman (1978), Bouchet et al. (1980) and Sicardy et al. (1982). Also, Bhattacharyya and Bappu (1977) and Bhattacharyya et al. (1979) have asserted that an extended, Saturn-like ring system surrounds Uranus. However, only nine rings have been confirmed. In fact, the occultation data place a limit of ~ 0.05 on the optical depth of any inter-ring material that lies anywhere from the top of the Uranian atmosphere to well beyond the orbit of Miranda. The imaging data place more stringent limits on the integrated amount of inter-ring material, as we discuss in Sec. IV.

II. RING STRUCTURE

A. Observed Characteristics

Enough optical depth profiles have been accumulated for us to characterize the ring structures and to conclude that the radial structure is not, in general, the same from occultation to occultation. Hence the ring structure must vary with orbital longitude or time or both. Below we describe the structures that have been observed for all of the nine rings. These structures are illustrated in Figs. 4 through 7 and summarized in Table II. (See also Table III for figure parameters.)

Rings 6, 5 and 4. These three rings are unresolved in all occultation observations to date, which suggests intrinsic radial widths ≤ 2 km. Lower limits on their widths in the range 0.4–0.8 km follow from the fraction of

1984prin.conf...25E

TABLE I

Observations of Occultations by the Uranian Rings

Date	Star[a]	Magnitude[b] V	K	V-K	Stellar Profile Angular Diameter[c] (milliarcsec)	FWHM at Uranus (km)	Sky Plane Velocity (km s^{-1})	Number of Sites	References[d]
10 Mar 1977	SAO 158687	9.0	5.2	3.8	0.55	6.5	17	6	1–8
23 Dec 1977	KM 2	10.4	7.0	3.4	0.24	2.9	27	1	9
4 Apr 1978	KM 4	13.4	11.9	1.5	0.024	0.3	18	1	10
10 Apr 1978	KM 5	11.6	10.1	1.5	0.055	0.6	20	1	10
10 Jun 1979	KM 9	13.7	11.0	2.7	0.037	0.4	19	1	11
20 Mar 1980	KM 11	13.0	10.1	2.9	0.057	0.7	10	1	12
15 Aug 1980	KM 12	12.3	8.7	3.6	0.11	1.3	8	3	13–16
26 Apr 1981	KME 13	10.0	7.4	2.6	0.19	2.2	20	2	17
22 Apr 1982	KME 14	11.6	5.2	6.4	0.54	6.1	18	5	18
1 May 1982	KME 15	11.4	7.4	4.0	0.20	2.3	21	1	18
4 Jun 1982	KME 16	13.0	9.5	3.5	0.075	0.8	22	1	18
3 Mar 1983	KME 17a	10.3	8.8	1.5	0.10	1.4	5	1	18
25 Mar 1983	KME 17b	10.3	8.8	1.5	0.10	1.3	5	2	18

[a]SAO refers to the Smithsonian Astrophysical Observatory Catalog; KM to the prediction list of Klemola and Marsden (1977); and KME to the prediction list of Klemola et al. (1981).

[b]Compiled by K. J. Meech from a variety of sources. The errors may be as large as a few tenths of a magnitude in some cases.

[c]Calculated by K. J. Meech, based on the data of Ridgway et al. (1980) and the magnitudes given here.

[d]References: 1. Elliot et al. (1977*a*, *b*); 2. Millis et al. (1977*a*, *b*); 3. Churms (1977); 4. Bhattacharyya and Kuppuswamy (1977); 5. Mahra and Gupta (1977); 6. Chen et al. (1978); 7. Elliot et al. (1978); 8. Hubbard and Zellner (1980); 9. Millis and Wasserman (1978); 10. Nicholson et al. (1978); 11. Nicholson et al. (1981); 12. Elliot et al. (1981*b*); 13. Elliot et al. (1981*a*); 14. Nicholson et al. (1982); 15. Sicardy et al. (1982); 16. Elliot et al. (1983); 17. French et al. (1982); 18. Unpublished.

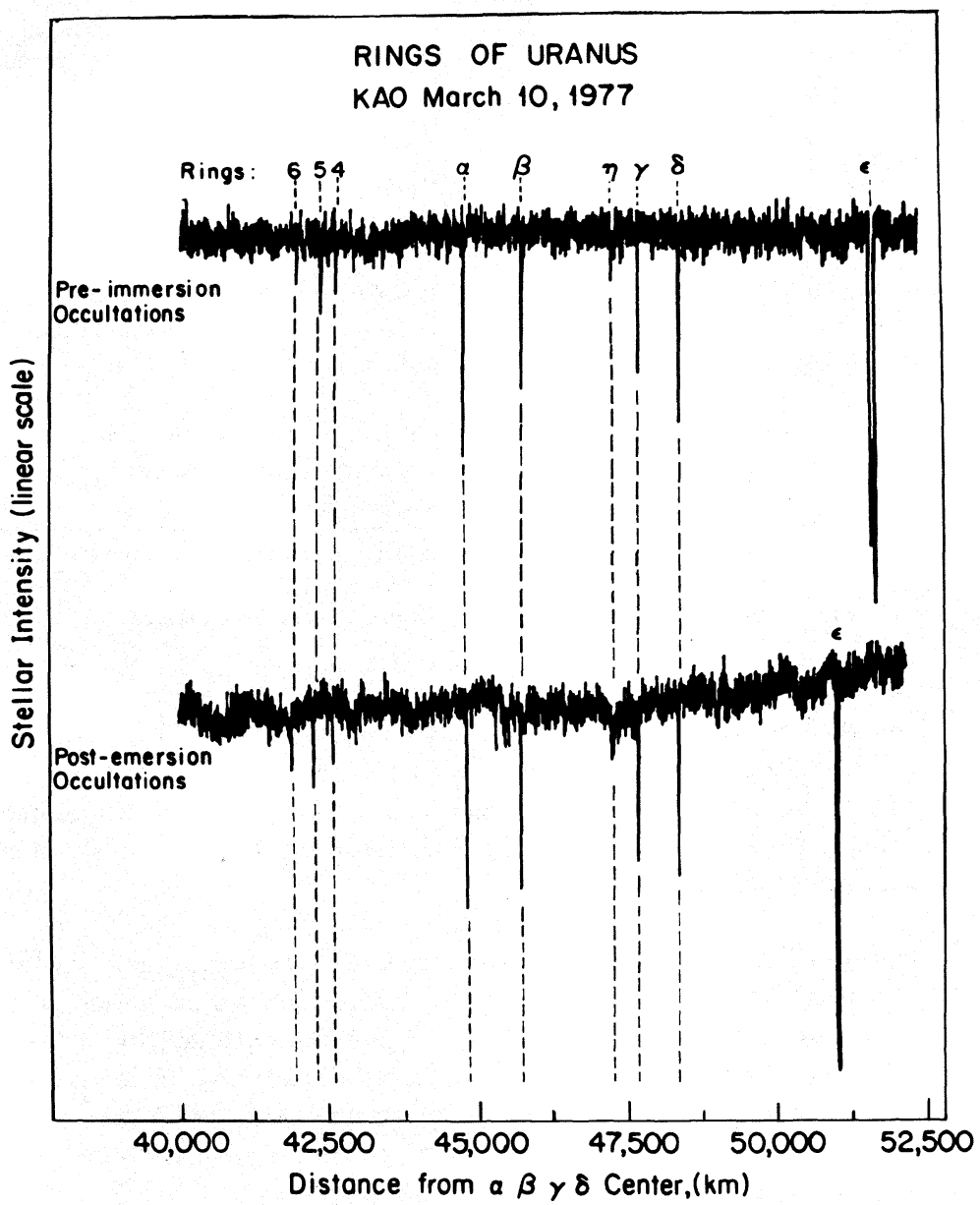

Fig. 3. Occultations by the rings of Uranus. The pre-immersion and post-emersion occultations by the rings of Uranus observed with the Kuiper Airborne Observatory (Elliot et al. 1977*c*) have been plotted on the common scale of distance from the center of Uranus in the ring plane. Occultations corresponding to the nine confirmed rings are easily seen. Most (if not all) of the low-frequency variations in the lightcurves are due to a variable amount of scattered moonlight on the telescope mirror (figure after Elliot 1979).

TABLE II

Ring Structures

Ring	Radial Width[a] (km)	Normal Optical Depth	Confirmed Structural Features
6	0.4–2	≥ 0.5	—
5	0.8–2	≥ 1.0	—
4	0.7–2	≥ 0.8	—
α	5→10	$\sim 1.4 \rightarrow 0.7$	"Double-dip" structure at widest part
β	$5 \rightarrow 11$	$\sim 1.5 \rightarrow 0.35$	—
η	0.5–2[b]	≥ 0.6[b]	Broad component terminated by a 2nd narrow ringlet ~55 km outside principal component
γ	~3	≥ 1.5	—
δ	2–3	≥ 1.5	2nd component ~12 km inside
ϵ	$20 \rightarrow 96$	$? \rightarrow 1.2$[c]	Consistent internal structure, sharp edges

[a]→ indicates established width variation, otherwise a range of possible widths is given.
[b]Narrow component.
[c]Optical depth of narrowest part of the ϵ Ring is too high to be reliably measured.

starlight that could be intercepted by a totally opaque ring. The integrated extinction of Ring 6 is somewhat less than that for Rings 5 or 4. There is little evidence for variations in extinction, although variations in width for all three rings might be expected by analogy with those established for the other eccentric rings (see below).

α Ring. This ring is almost always resolved, and varies in width by a factor of ~2. At its maximum width of ~10 km, on two occasions, it has shown a "double-dip" structure: two components separated by ~4 km, which is essentially at the limit of our spatial resolution. This could be indicative either of a structured ring or of an internal division that extends around the ring, but is resolved only where the ring is widest. At its widest part, the average normal optical depth of the α Ring is ~0.7 (Nicholson et al. 1982).

β Ring. This ring is also almost always resolved, and exhibits a range of widths similar to that of the α Ring. It shows, however, no evidence of internal structure except for a possible difference in the sharpness of the inner and outer edges. The average normal optical depth at the widest part of the β Ring is ~0.35, which suggests that it may contain about half as much material as the α Ring. This conclusion is supported below by an analysis of the width variations of both rings.

TABLE III

Parameters for Ring Profiles[a]

Ring	Figure in text	Zero-point Radius (km)	True Anomaly[b] (deg)	Radial Velocity (km s^{-1})
6	4	41872	276.7	8.29
5	4	42293	103.5	8.29
4	4	42634	239.8	8.30
α	5	44792	193.1	8.34
β	5	45713	132.1	8.36
η	4,6	47216	(142.4)	8.39
γ	5	47667	(262.0)	8.39
δ	5	48337	316.3	8.40
ϵ	7	51279	256.7	8.45

[a]These parameters refer to the Cerro Tololo Inter-American Observatory profiles and would be slightly different for the European Southern Observatory and Las Campanas Observatory profiles. (See Figs. 4–7.)

[b]Angle from periapse.

η Ring. This ring comprises both a narrow, unresolved component (see Fig. 4) and a broad (~55 km) component of low optical depth that is located primarily, and perhaps entirely, outside the narrow component. The optical depth of the broad component apparently varies considerably, with measured values ranging from ~0.03 to ~0.10, as shown in Fig. 6. A second unresolved sharp feature occurs at or near the outer edge of the broad component. The η Ring appears strikingly similar to the F Ring of Saturn (Lane et al. 1982), since they each have broad and narrow components of about the same widths and optical depths. One difference, however, is that the narrow component of the η Ring lies at the inner edge of the broad component while for the F Ring the situation is reversed. In this regard, it might prove significant that the radius of the η Ring is smaller than the corotation radius, while the radius of the F Ring is larger than the corotation radius.

γ Ring. This ring lies at the limit of our spatial resolution, and is probably ~3 km in width and fairly opaque ($\tau \gtrsim 1.5$). It appears to have very sharp edges, judging from the frequently prominent diffraction fringes on the occultation profiles.

δ Ring. Although very similar in its occultation signature to the γ Ring, the δ Ring may be slightly narrower and/or less opaque. Its diffraction fringes are generally less prominent than those of the γ Ring. It now appears probable that this ring also has a secondary component, in this instance located ~12 km inside, and with an integrated extinction ~10% of the primary component.

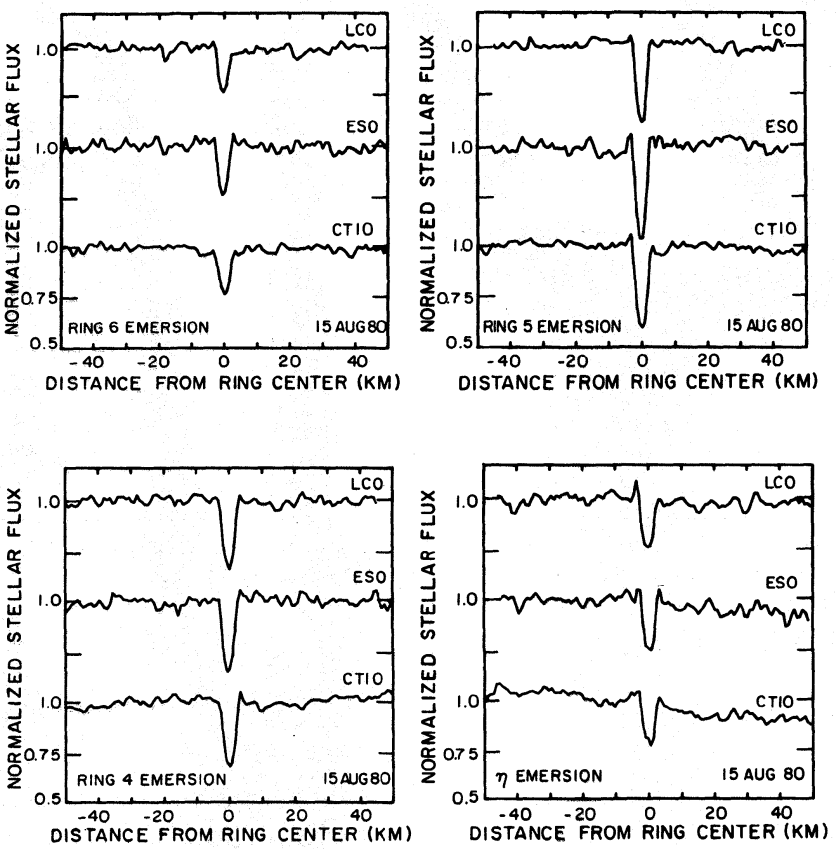

Fig. 4. Occultation profiles of Rings 6, 5, 4 and the narrow component of the η Ring. Here and in Fig. 5 the emersion data obtained from Las Campanas, the European Southern Observatory and Cerro Tololo on 15–16 August 1980 have been aligned according to their midradii. The width of each of these profiles is near the diffraction limit. See Table III for zero-point radius (figure after Elliot et al. 1983).

ϵ Ring. This ring, with a width varying from 20 to 96 km (see below), is always well resolved and shows considerable structural detail (see Fig. 7). This structure is largely consistent from one occultation to another, except possibly for the narrowest profiles, which are essentially featureless and correspond to large optical depths. (Six representative observations of the ϵ Ring, reproduced at a uniform radial scale, are presented in Fig. 8b.) The outer third of the ring consistently has the highest average optical depth, with a secondary maximum occurring at or near the inner edge. There are no resolved gaps within the ring, although the presence of numerous unresolved gaps seems quite likely. Both inner and outer edges are sharp, and frequently show low amplitude diffraction fringes. The average optical depth of the ϵ Ring is ~ 1.2 at its widest part, and varies approximately inversely with ring width (see Table IV).

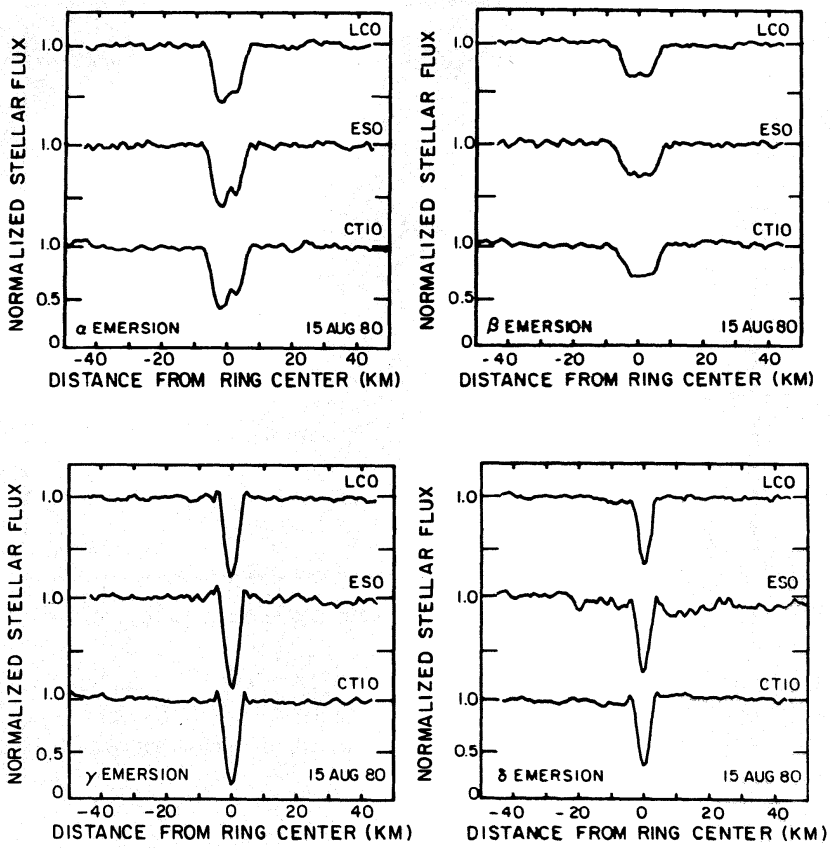

Fig. 5. Occultation profiles of Rings α, β, γ and δ (cf. Fig. 4). Note the "double-dip" structure of the α Ring, the lack of structure in the β Ring and the diffraction fringes on the γ Ring. See Table III for zero-point radius (figure after Elliot et al. 1983).

TABLE IV

Parameters for ϵ Ring Profiles[a]

Profile	Date I=Immersion E=Emersion	Site[b]	Zero-point Radius (km)	True Anomaly (deg.)	Radial Velocity (km s^{-1})	Radial Width[c] (km)
a	4/10/78 I	LCO	50789	9.2	18.65	20.5
b	4/10/78 E	LCO	51353	113.9	18.79	76.5
c*	4/22/82 I	LCO	51504	141.9	17.49	88.7
d	3/10/77 I	PO	51594	182.5	12.28	98.2
e	8/15/80 E	LCO	51278	256.8	8.44	68.0
f*	4/22/82 E	LCO	51086	284.3	17.63	46.5

[a]See Fig. 8 in Sec. II.C.

[b]LCO = Las Campanas Observatory, Chile;
PO = Perth Observatory, Australia.

[c]The widths plotted in Fig. 10 are based on a previous analysis and some may differ by up to 2 km from the values presented in this table. Those in the table are preferred.

*Since these data were not included in the orbit solution of Table VI, their zero-point radii, true anomalies and radial velocities may change, relative to the other data, when the fitted orbit model is updated to include these points.

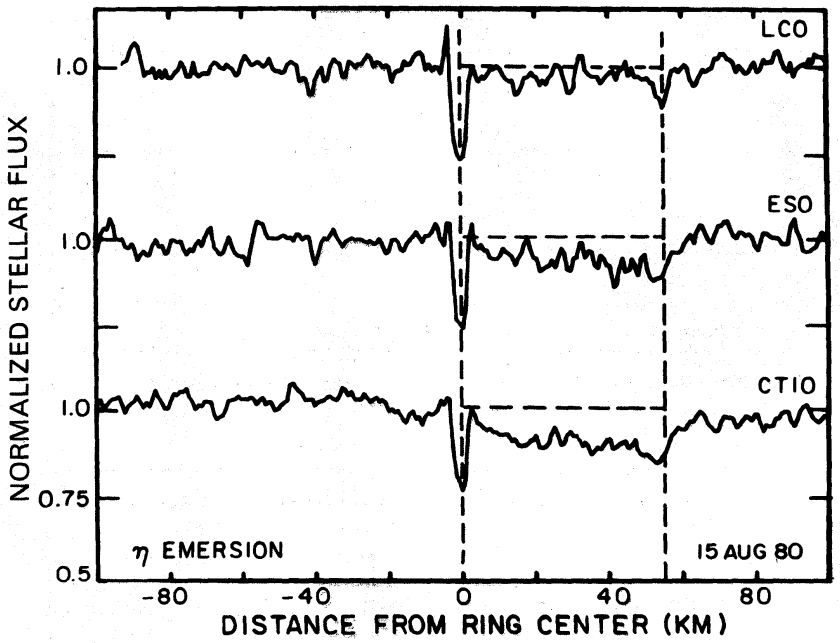

Fig. 6. A comparison of η Ring profiles from Las Campanas, the European Southern Observatory and Cerro Tololo obtained on 15–16 August 1980. Note the different occultation depths obtained at the three observatories. See Table III for zero-point radius (figure after Elliot et al. 1983.)

B. Model Profiles

From the above discussion, we see that the structures of most rings cannot be described by a simple model. However, deconvolution of the actual profiles from the data is not possible because we lack the phase of the detected light and have limited signal-to-noise ratio. While not the ideal solution to these problems, the fitting of simple models to the profiles does yield certain information. First, it provides a consistent method for obtaining the mid-times of ring occultations, which are needed to determine the ring orbits (see Sec. III). Second, model fitting is also a consistent method for defining the ring widths.

Two types of model have been fitted to the data. The first is a trapezoid model, which includes the effects of a finite star diameter and the time constant of the data recording system, but not diffraction (Elliot et al. 1981*b*). The second model treats the optical depth profile of the ring as a "square well" of uniform, nonzero transmission and includes the effects of diffraction, the passband of the filter, the stellar diameter and the time constant of the data-recording equipment (Nicholson et al. 1982). A typical model ring profile at various stages of the calculation is shown in Fig. 9. The above conclusions concerning intrinsic ring widths and optical depths are based on such modeling.

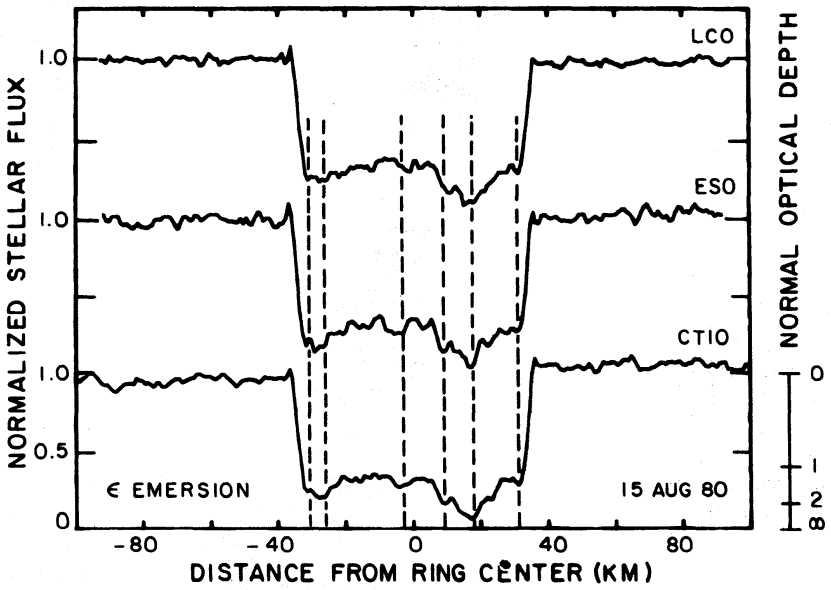

Fig. 7. A comparison of ϵ Ring profiles from Las Campanas, the European Southern Observatory and Cerro Tololo on 15–16 August 1980. Coincident features in the three profiles, most of which correspond to those pointed out by Nicholson et al. (1982), have been highlighted by dashed lines. See Table III for zero-point radius (figure after Elliot et al. 1983).

C. Width-Radius Relationships

The systematic variation in radial width of the ϵ Ring provided the first clue that at least one of the Uranian rings was eccentric. Nicholson et al. (1978) discovered a linear relation between the width and radius of different segments of this ring. Such a relation is expected for an eccentric ring whose inner and outer edges have slightly different eccentricities but the same longitude of periapse (see below). Subsequently, similar width-radius relations were established for the α and β Rings (Elliot et al. 1981*b*; Nicholson et al. 1982). Figs. 10–12 show these relations, revised to include the 1981 and 1982 observations.

Although this eccentric model is clearly in good agreement with the observations, especially for the ϵ Ring, differential apsidal precession between the inner and outer edges of each ring due to Uranus' oblate figure amounts to 180° in only a few hundred years. Rapid disruption and circularization of initially eccentric rings is thus inevitable, unless some mechanism exists to cancel the differential component of precession. Goldreich and Tremaine (1979*b*) have shown that this can be accomplished by the rings' self-gravity, although other possibilities also exist (Dermott and Murray 1980).

A uniformly precessing, eccentric ring can be described in terms of a set of nested, nonintersecting ring particle orbits, much like the streamlines of laminar fluid flow. Each orbit is a Keplerian ellipse with a certain semimajor axis a, eccentricity e, and longitude of periapse ϖ. All orbits share the same

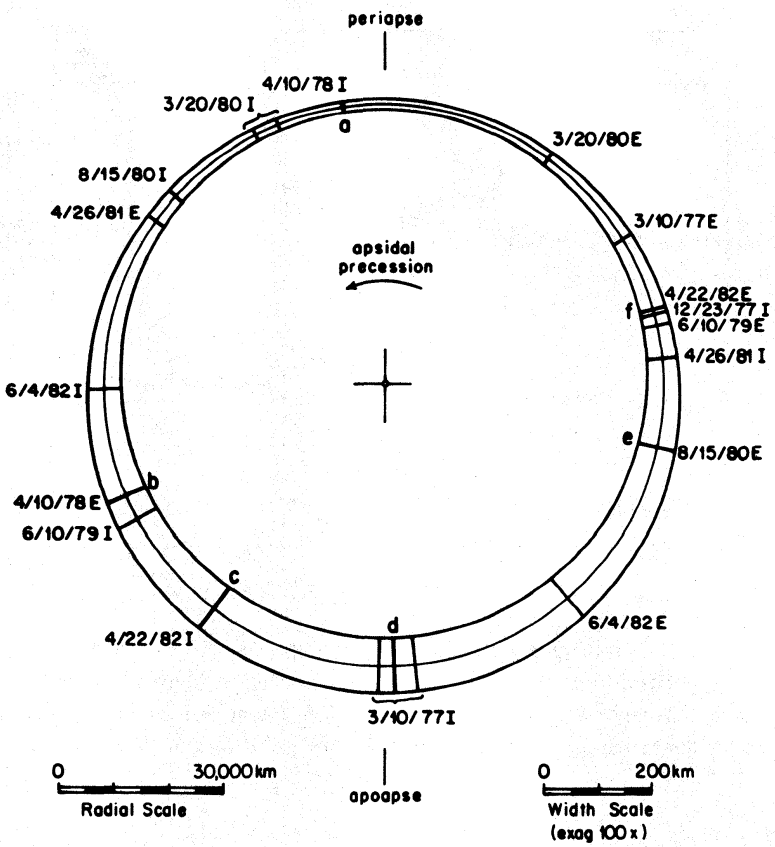

Fig. 8a. A diagram of the ϵ Ring, viewed from above Uranus' north pole, showing the locations of the various stellar occultation profiles. Note that the width of the ring is exaggerated by a factor of 100 for purposes of clarity, but that the center line of the ring is plotted with the correct eccentricity of 0.0079.

apsidal precession rate $\dot{\varpi}$, but there is a gradient (across the ring) of e, and possibly of ϖ as well. In terms of the total ranges in a, e and ϖ from the inner to the outer edge of the ring (δa, δe and $\delta\varpi$), the radial width of the ring as a function of azimuth θ, measured from the mean periapse, is

$$\begin{aligned} w &\simeq (1 - q_e \cos\theta - q_\omega \sin\theta)\, \delta a \\ &= (1 - Q \cos(\theta - \theta_0))\, \delta a \end{aligned} \tag{1}$$

where $q_e = a\delta e/\delta a$, $q_\omega = ae\delta\varpi/\delta a$, $Q = (q_e^2 + q\omega^2)^{\frac{1}{2}}$, and $\tan\theta_0 = q_\omega/q_e = e\delta\varpi/\delta e$. This expression is derived under the simplifying, but quite valid, assumptions that $\delta e \ll e \ll 1$, $\delta a \ll a$, $\delta\varpi \ll \pi/2$, and $\delta a/a \ll \delta e/e$. To $\mathcal{O}(e)$, the mean radius of the ring is given by $r = a\,(1 - e\cos\theta)$, where a and e are the mean semimajor axis and eccentricity, so that if $\delta\varpi = 0$ we have the linear relation:

$$w = \delta a + \frac{\delta e}{e}(r - a). \tag{2}$$

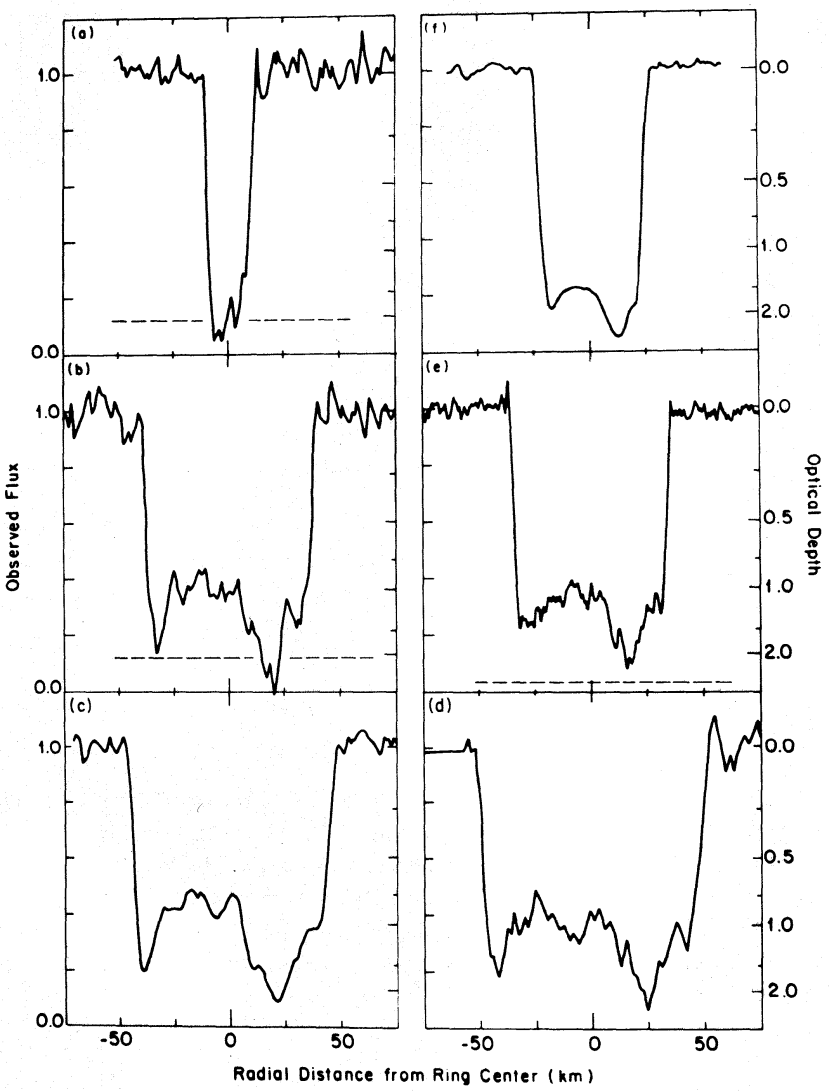

Fig. 8b. Six representative occultation profiles of the ϵ Ring, corresponding to observations (a-f) in Fig. 8a, plotted at a uniform radial scale. Details of the particular observations may be found in Table IV. The ordinate is observed flux, normalized to the average flux levels immediately preceding and following the event. Except for the March 1977 profile, no attempt has been made to subtract the small, but rather uncertain, contributions of Uranus and the rings to the total flux. Dashed lines indicate the upper limits to these contributions, where they are $>1\%$ of the stellar flux. The unusually smooth appearance of the April 1982 profiles (c and f) is due, in part, to the rather large angular diameter of the occulted star (see Table I). The data is from Millis et al. (1977*a*), Nicholson et al. (1978, 1982), and K. Matthews (April 1982, unpublished).

From these relations, and from the linear fits to the observed widths in Figs. 10–12, values of δa and δe have been obtained for the α, β and ϵ Rings and are given in Table V. Mean values of a and e are taken from the kinematic models in Table VI. Also given are the inferred minimum and maximum

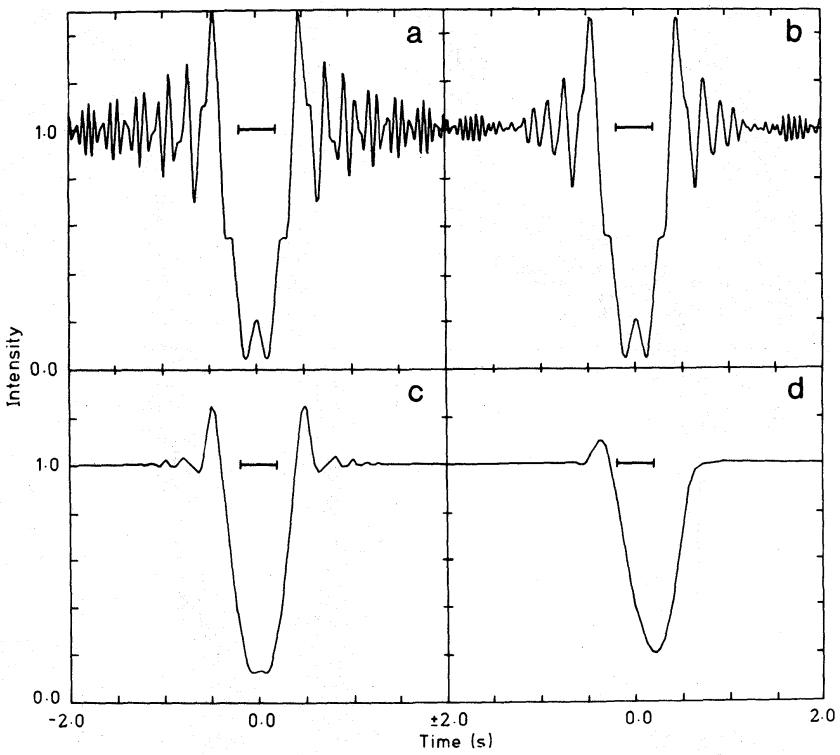

Fig. 9. Successive steps in the generation of a synthetic occultation profile for an opaque ring with a projected width of 3.0 km. The geometric shadow of the ring is indicated by a horizontal bar, and the velocity of the shadow relative to the observer is 7.5 km s^{-1}. (a) Monochromatic ($\lambda = 2.2$ μm) diffraction pattern for a point source; (b) averaged over the 2.0–2.4-μm passband; (c) convolved with the intensity distribution of a uniform circular source of angular diameter 1.3×10^{-4} arcsec; (d) convolved with the instrumental response function (figure after Nicholson et al. 1982).

widths, $\delta a(1-q_e)$ and $\delta a(1+q_e)$. Strictly speaking, these widths are FWHM occultation profile widths and are larger than the intrinsic ring widths by 0.5–1.0 km.

In the future, with an improved data base, it may be possible to determine $\delta\tilde{\omega}$ from the distribution of ring widths with orbital longitude. We note that the effect of a small deviation in longitude of periapse between the inner and outer edges of an eccentric ring is to produce a much larger (by a factor of $e/\delta e$) offset in the longitude of minimum ring width from the mean longitude of periapse. Such an offset has been discussed by Dermott and Murray (1980) in connection with the development of the eccentricity gradient across the ϵ Ring. Measurement of a nonzero $\delta\tilde{\omega}$ could provide information on dissipative processes operating within the rings.

The mechanism by which the α, β and ϵ Rings are maintained in a state of uniform precession is uncertain, but the simplest and most readily quantified model is that of Goldreich and Tremaine (1979*a*), who attribute the necessary small perturbations to the "free" precession rates (i.e., those in-

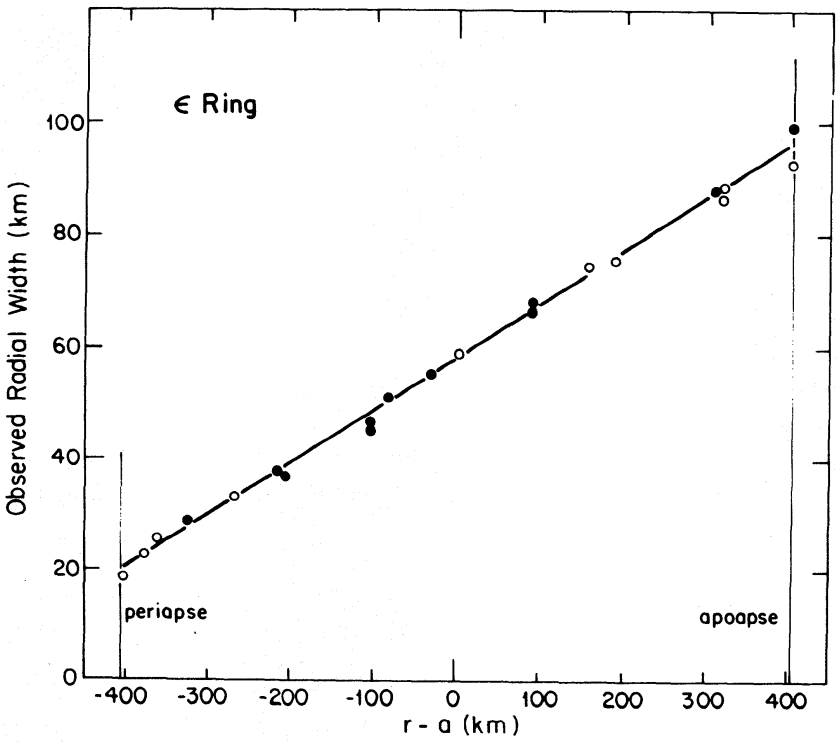

Fig. 10. Relation between radial width (occultation profile FWHM projected onto the radial direction in the ring plane) and the center-line radius exhibited by the ϵ Ring, including data from 8 stellar occultations (see Fig. 8a, b). The zero of the radius scale is the semimajor axis of the ring, as given in Table VI. Open and filled symbols indicate ring segments whose true anomalies (i.e., angles from periapse) lie in the respective ranges 0°–180° and 180°–360°. The line is a linear least-squares fit of Eq. (2) to the data, the resulting values of δa, δe and q_e being given in Table V. Deviations of individual points from the fitted relation are no more than a few km in radial width, comparable to the uncertainties in the measurements.

duced by Uranus) to the self-gravity of the rings. One prediction of this model is that the eccentricity gradient q_e must be positive, as observed. A second consequence is a relation between the total mass of each ring and the parameters δa and δe:

$$m_{\text{ring}}/M_u = \frac{21\pi}{8} f \frac{e}{\delta e} \left(\frac{\delta a}{a}\right)^3 J_2 \left(\frac{R}{a}\right)^2 \tag{3}$$

where J_2 is the usual coefficient in the zonal harmonic expansion of Uranus' gravitational field, R is the equatorial radius of Uranus, and f is a dimensionless factor which depends on the distribution of mass within the ring. Generally, $f \simeq 0.5$ (Goldreich and Tremaine 1979*a*,*b*). From this expression, and the value of J_2 derived from kinematic models of the rings in Sec. III, the ring masses and average surface densities σ given in Table V are derived. Note that the mass obtained for the α Ring is ~50% greater than that obtained for the β Ring, and that the inferred minimum surface densities, corresponding to

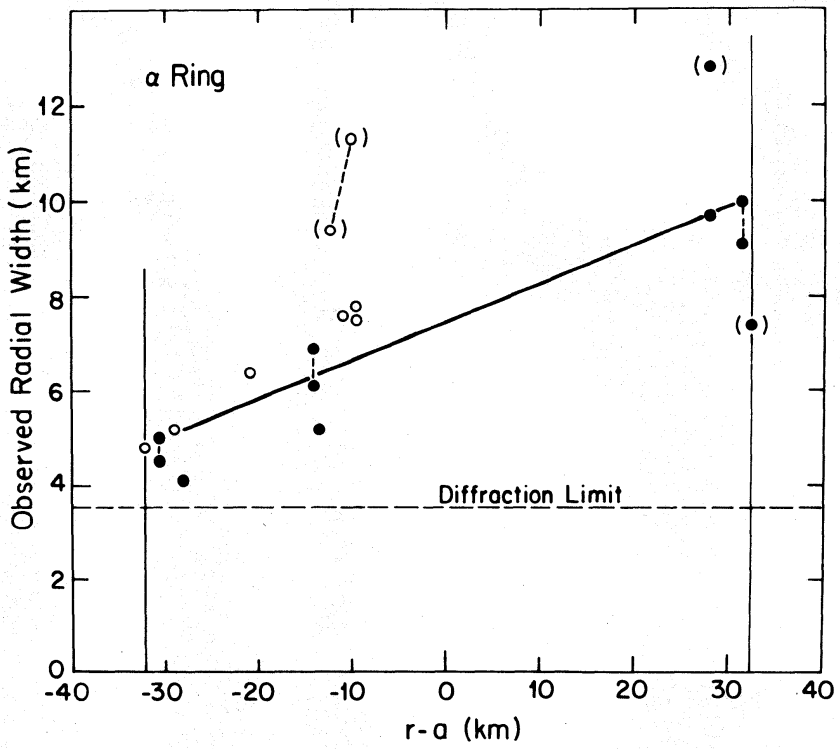

Fig. 11. Width-radius relation for the α Ring, with symbols as in Fig. 10. Multiple observations of the same event from nearby stations are connected by dashed lines. The horizontal dashed line represents the minimum FWHM, set by diffraction, of ~3.5 km at a wavelength of 2.2 μm. As in Fig. 10, the zero of the radius scale is the semimajor axis of the ring, given in Table VI. In constructing the linear least-squares fit of Eq. (2) to the data, the obviously discrepant points shown in parentheses have been discarded. (These discrepancies, which do not appear to be attributable to observational uncertainties or error, suggest that the structure of the α Ring is more complicated than the present simple model.) Values of δa, δe and q_e derived from the fit are given in Table V.

maximum widths, are in approximate proportion to the optical depths given above. In each case, the opacity, defined as τ/σ, is ~0.8 cm^2 g^{-1}. The implied mass of the ϵ Ring is much greater, and it seems likely that this ring contains ~99% of the total mass in the system. The opacity derived for the ϵ Ring, 0.08 cm^2 g^{-1}, is significantly lower than that obtained for α and β, as pointed out by Yoder (1982). This suggests a somewhat larger mean particle size for the ϵ Ring. In comparison, the opacity of Saturn's A and B Rings, as inferred from the study of density waves (see chapter by Cuzzi et al.), is ~0.01 cm^2 g^{-1} in most regions where it has been measured. Analyses of two narrow, eccentric ringlets in Saturn's C Ring yield opacities of 0.05 cm^2 g^{-1} (Esposito et al. 1983; Porco et al. 1983), comparable with that of the ϵ Ring.

Finally, we note that a similar argument about disruption by differential precession applies to inclined rings, so that for such rings the nodal line must regress uniformly. According to the self-gravity model, such uniform regression must be accompanied by gradients in inclination across the ring, with $\delta i/i$

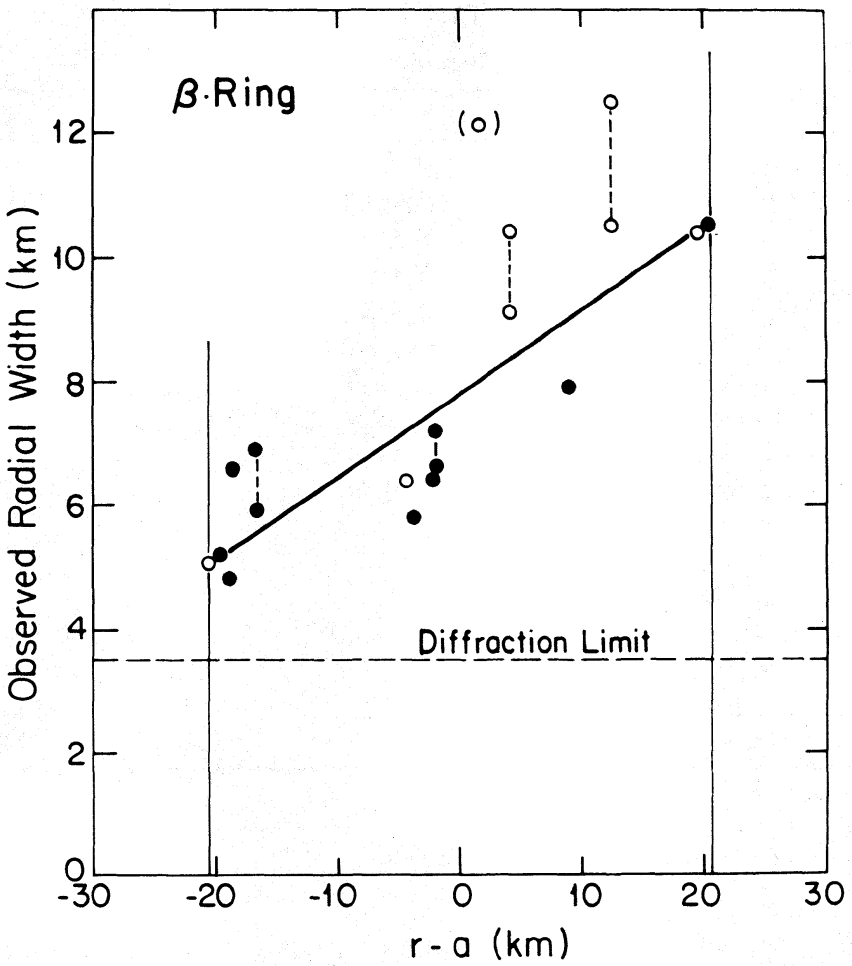

Fig. 12. Width-radius relation for the β Ring, with symbols as in Figs. 10 and 11. Note that the total range in radial width for the β Ring is comparable to that shown by the α Ring, although the eccentricity of β is significantly lower (see Table VI). Only one discrepant point, shown in parentheses, has been omitted from the least-squares fit of Eq. (2) to the data, the results of which are given in Table V.

$\simeq \delta e/e$ (Borderies et al. 1983). It may be possible to detect such gradients by their effects on the projected widths of the inclined rings (see Sec. III), although the present near pole-on aspect of the system reduces the predicted amplitude of the effect to $\lesssim 1$ km for any of the rings.

III. RING ORBITS

A remarkable feature of the Uranian rings is the high precision with which we can derive their orbits from multiple occultation observations. From each event we obtain a large number of points on the ring orbits whose relative positions are precisely known. The situation is illustrated in Fig. 13 for the discovery occultation on 10 March 1977. The basic reason for the high precision of the orbital parameters is the high precision of the occultation data; but

TABLE V

Width-Radius Relations and Ring Masses

Ring	α	β	ϵ
Directly Measured Parameters			
a (km)[a]	44758	45701	51188
δa (km)	7.5 ± 0.2	7.8 ± 0.3	58.0 ± 0.4
e[a]	7.8×10^{-4}	4.3×10^{-4}	7.94×10^{-3}
δe	5.8×10^{-5}	6.0×10^{-5}	7.4×10^{-4}
$q_e = a\delta e/\delta a$	0.35 ± 0.03	0.35 ± 0.05	0.65 ± 0.01
Minimum width (FWHM, km)	4.9	5.0	19.8
Maximum width (FWHM, km)	10.1	10.6	96.3
Normal optical depth at maximum width, τ_0	0.7[b]	0.35[b]	1.2[c]
Parameters Inferred From Goldreich and Tremaine Model			
Total mass (g)	2.6×10^{16}	1.4×10^{16}	4.9×10^{18}
Average surface density σ(g cm^{-2})	1.2	0.65	26
σ at maximum width σ_0 (g cm^{-2})	0.9	0.5	16
Opacity $= \tau_0/\sigma_0$ (cm^2 g^{-1})	0.8	0.8	0.08

[a]From kinematic models. See Table VI.
[b]Nicholson et al. (1982). See Table II.
[c]Integrated optical depth/FWHM at maximum width.

another important factor is that the pole of Uranus is only 8° from its orbit plane. Hence, we see the rings from a continuously changing aspect that goes through a complete cycle during an orbit period of about 84 yr. In 1986 the ring system will appear almost pole-on to the Earth. A fundamental difference exists between determining satellite orbits and ring orbits from Earth-based observations: for satellite orbits we know the revolution period more precisely than the orbit dimensions; for ring orbits we know the dimensions precisely, but can measure only their precession periods—not their revolution periods.

The kinematic model has been developed through a series of papers (Elliot et al. 1978, 1981*a*, *b*; Nicholson et al. 1978, 1981, 1982; French et al. 1982) into its present state. The model treats the rings as ellipses, which are inclined to the equatorial plane of Uranus and precessing under the influence of the zonal harmonics of Uranus' gravitational field. Both apsidal and nodal precession rates are assumed to be uniform across each ring, for the reasons discussed in the previous section. Hence it is only necessary to fit the orbit of the center of mass of each ring (approximated by its center line), rather than the two edges separately. The uniform ring precession rates are taken to be the rates appropriate to an infinitely narrow ring located at the center line.

The origin of the apsidal and nodal precession can be understood most readily in terms of the three natural angular velocities of particle motion about

1984prin.conf...25E

TABLE VI

Fitted Model Parameters: Orbital Elements[a]

Ring	Semimajor Axis a (km)	Eccentricity $e \times 10^3$	Azimuth of Periapse $\tilde{\omega}_0$ (deg)[b]	Inclination i (deg)	Azimuth of the Ascending Node Ω_0 (deg)[b]
6	41877.3 ± 16.6	1.01 ± 0.10	243.6 ± 3.6	0.066 ± 0.012	15.7 ± 4.4
5	42275.2 ± 16.6	1.85 ± 0.08	170.1 ± 2.5	0.050 ± 0.010	288.5 ± 9.1
4	42609.6 ± 16.8	1.15 ± 0.04	125.3 ± 3.0	0.022 ± 0.005	117.2 ± 24.7
α	44758.3 ± 16.4	0.78 ± 0.02	329.4 ± 2.3	0.017 ± 0.003	65.4 ± 13.6
β	45701.0 ± 16.5	0.43 ± 0.02	223.9 ± 2.8	0.006 ± 0.002	296.3 ± 41.0
η	47214.9 ± 16.5	(0.03 ± 0.04)[d]	(129.0 ± 58.0)	(0.003 ± 0.004)	(263.0 ± 117.7)
γ	47666.3 ± 16.4	(0.04 ± 0.02)	(84.0 ± 22.3)	0.006 ± 0.002	100.2 ± 31.1
δ	48338.7 ± 16.5	0.06 ± 0.02	135.1 ± 15.8	0.012 ± 0.003	299.0 ± 11.5
ϵ	51188.1 ± 17.0	7.94 ± 0.02	214.9 ± 0.4	(0.003 ± 0.003)	(242.9 ± 29.5)

Harmonic Coefficients of the Gravity Potential[c]

$J_2 = (3.349 \pm 0.005) \times 10^{-3}$

$J_4 = (-3.8 \pm 0.9) \times 10^{-5}$

Pole of the Ring Plane

$\alpha_{1950.0} = 5^h\,06^m\,29^s.4 \pm 5^s.3$

$\delta_{1950.0} = +15°\,14'\,10'' \pm 1'31''$

[a] For $M_u = 8.669 \times 10^{28}$ gm and $G = 6.670 \times 10^{-8}$ dyn cm^2 gm^{-2}; this tabulation is for the model of French et al. (1982).

[b] At 20:00 UT on 10 March 1977.

[c] For a reference radius, $R = 26{,}200$ km.

[d] Those eccentricities, inclinations, and associated angles within parentheses cannot be distinguished from zero.

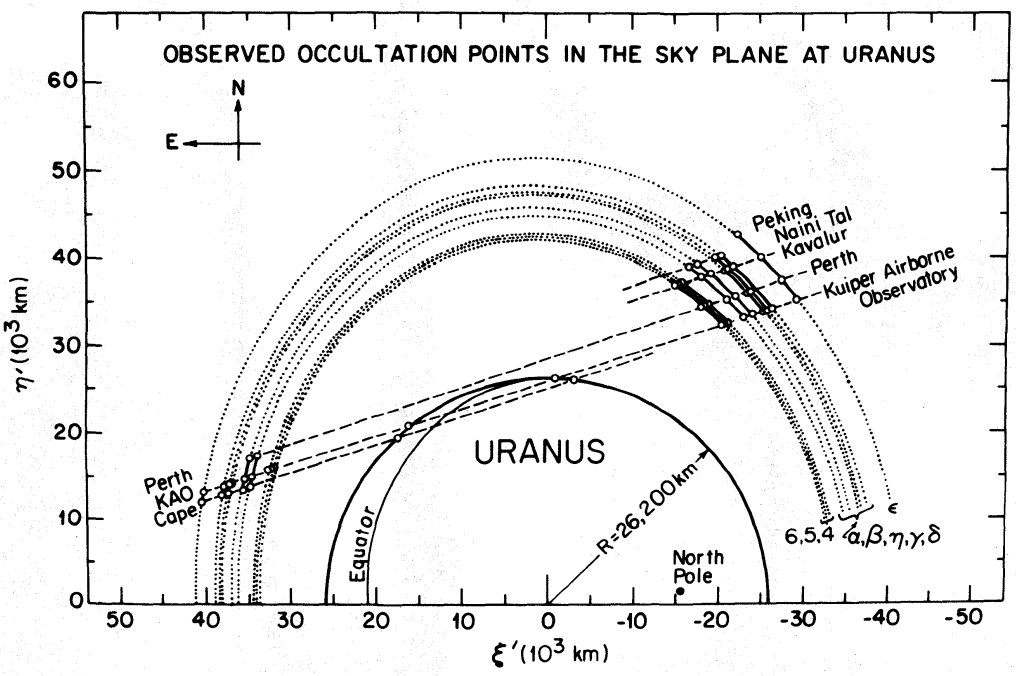

Fig. 13. Observed occultation points in the sky plane at Uranus for the 10 March 1977 occultation of SAO 158687. The observed points are indicated by open circles, pre-immersion points to the *right* and post-emersion points to the *left*. The dashed lines show the tracks of the observatories in the sky plane. The rings are indicated by dotted lines and the solid segments between the observed occultation points. The radius of Uranus corresponds to a number density level of 6×10^{13} cm^{-3} (figure after Elliot et al. 1978).

an oblate planet: the mean angular velocity* of the orbital motion n; the mean angular velocity of radial oscillations for a particle slightly displaced from a circular orbit κ; and the mean angular velocity* of vertical oscillations for a particle slightly displaced from the planet's equatorial plane ν. In terms of the mass and equatorial radius of the planet M and R and the usual zonal gravity harmonic coefficients J_2 and J_4, these three angular velocities are given by the following expressions, correct to first order in orbital eccentricity and inclination for terms involving J_2, J_2^2 and J_4:

$$n = \left(\frac{GM}{a^3}\right)^{\frac{1}{2}} \left[1 + \tfrac{3}{4} J_2 \left(\frac{R}{a}\right)^2 - \tfrac{9}{32} J_2^2 \left(\frac{R}{a}\right)^4 - \tfrac{15}{16} J_4 \left(\frac{R}{a}\right)^4\right] \tag{4}$$

$$\kappa = \left(\frac{GM}{a^3}\right)^{\frac{1}{2}} \left[1 + \tfrac{3}{4} J_2 \left(\frac{R}{a}\right)^2 - \tfrac{9}{32} J_2^2 \left(\frac{R}{a}\right)^4 - \tfrac{45}{16} J_4 \left(\frac{R}{a}\right)^4\right] \tag{5}$$

$$\nu = \left(\frac{GM}{a^3}\right)^{\frac{1}{2}} \left[1 + \tfrac{9}{4} J_2 \left(\frac{R}{a}\right)^2 - \tfrac{81}{32} J_2^2 \left(\frac{R}{a}\right)^4 - \tfrac{75}{16} J_4 \left(\frac{R}{a}\right)^4\right]. \tag{6}$$

*The units of "angular velocity" are radians/seconds.

Since $n > \kappa$, the longitude of periapse, measured from some inertially fixed direction, advances at a rate*

$$\dot{\varpi} = n - \kappa = \left(\frac{GM}{a^3}\right)^{\frac{1}{2}} \left[\tfrac{3}{2} J_2 \left(\frac{R}{a}\right)^2 - \tfrac{15}{4} J_4 \left(\frac{R}{a}\right)^4\right] . \quad (7)$$

Similarly, the longitude of the node regresses at a rate

$$\dot{\Omega} = n - \nu = -\left(\frac{GM}{a^3}\right)^{\frac{1}{2}} \left[\tfrac{3}{2} J_2 \left(\frac{R}{a}\right)^2 - \tfrac{9}{4} J_2^2 \left(\frac{R}{a}\right)^4 - \tfrac{15}{4} J_4 \left(\frac{R}{a}\right)^4\right] . \quad (8)$$

The fixed reference direction is chosen as the ascending node of Uranus' equatorial plane on the Earth's equator of 10 March 1977, 20^h UT.

In Eqs. (4) through (8), the quantity a is the *geometrical* semimajor axis of the ring, i.e., the semimajor axis of the best fitting ellipse traced by the ring particles. The deviation of the ring from an ellipse due to the harmonics of the Uranian potential would be order $ae^2 J_2 (R/a)^2$, only ~0.003 km for the ϵ Ring. Although a 2nd-order analysis is adequate for the instantaneous geometry of the rings, the secular effects of the precessions will require a 3rd-order treatment within the next few years. This will introduce terms in Eqs. (7) and (8) of order J_2^3, $e^2 J_2$, $J_2 J_4$, $i^2 J_2$, J_3 and J_6. The required expressions can be obtained by extending the analysis of Brouwer (1946) to the next order.

As discussed by Greenberg (1981), equivalent forms of Eqs. (7) and (8) have been written in terms of the osculating Keplerian elements (Brouwer 1959) and in terms of the observables (n and a) for satellite orbits (Kozai 1959; Brouwer 1946; Null et al. 1981). These three forms differ in the numerical coefficient of the J_2^2 term, since our a is not the osculating Keplerian semimajor axis and $n \neq (GM/a^3)^{\frac{1}{2}}$ (see Eq. 4).

These equations are the only dynamics included in the present kinematic model; the rest of the job just involves being careful with geometry. The method basically follows Smart's (1977) procedure, except that it becomes conceptually easier to project the occultation points into a three-dimensional coordinate system at Uranus instead of using Smart's fundamental plane that passes through the center of the Earth. Details of the method are discussed by Elliot et al. (1978, 1981*b*) and French et al. (1982).

We summarize the steps in the procedure as follows. First, the midtimes of the ring occultations are determined by either fitting a model profile or finding the midtime between the half-maximum signal points on the occultation profile. Next, the ephemerides of Uranus *and the star* are calculated, including the effects of precession and nutation but not stellar aberration, and these data are used to calculate coordinates and velocities (relative to the center of Uranus) for the star at the occultation times. This information is then available to a least-squares fitting program that minimizes the sum of the

*This rate is also denoted by $\dot{\pi}$ in the literature.

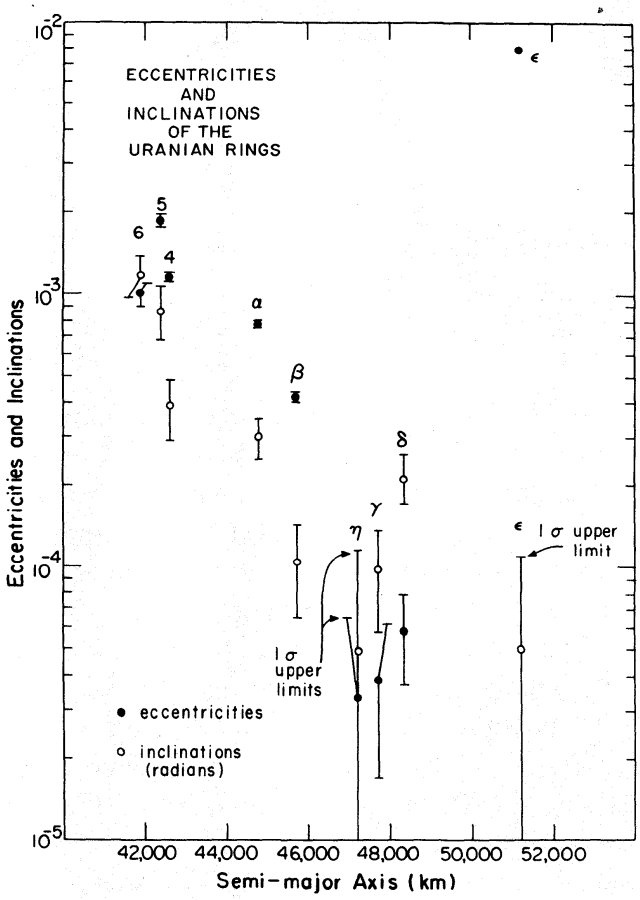

Fig. 14. Eccentricities (●) and inclinations (○) of the Uranian rings. The eccentricity and inclination (in radians) for each of the nine presently known rings are plotted against the semimajor axis. Except for the eccentricity of the ϵ Ring, the e's and i's show a decreasing trend with increasing semimajor axis. The eccentricities of the η and γ Rings, as well as the inclinations of the η and ϵ Rings, are not large enough to be statistically significant (figure after French et al. 1982).

squared residuals (in time) between the data and the orbit model. In accordance with our geometrical definition of the semimajor axis, the eccentricity e and inclination i (relative to Uranus' equatorial plane) are also defined in terms of the inclined ellipse traced by the ring particles. The free parameters in the final solution are:

1. a, e, and i for each ring;
2. The longitude of periapse (ϖ_0) and the longitude of the ascending node (Ω_0) for each ring at a specified epoch (10 March 1977 at 20^h UT);
3. The right ascension and declination (α_p and δ_p) for the rotation pole of Uranus;
4. J_2 and J_4 for Uranus;
5. Corrections in right ascension and declination ($\Delta\alpha$ and $\Delta\delta$) to the coordinates of each occulted star.

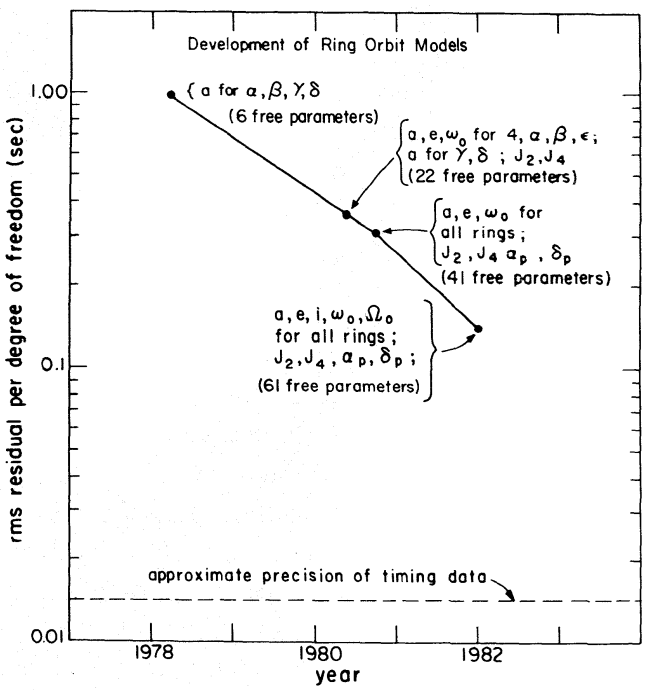

Fig. 15. Development of ring orbit models. As the model has been made more realistic by including more parameters, the rms error per degree of freedom has decreased. However, the rms error of the present model is still substantially larger than the timing errors in the data, indicating that the model is not yet complete.

The most recent model, incorporating data through April, 1981, fits 61 parameters to 140 data points and is given in Table VI, where the errors are the formal errors in the parameters from the least-squares fit. One interesting relation between the orbit parameters is shown in Fig. 14, where the eccentricity and inclination of each ring is plotted versus its semimajor axis. Except for the eccentricity of the ϵ ring, we see a generally decreasing trend of the eccentricities and inclinations as the semimajor axis increases. This effect may or may not prove significant, and no explanation has been proposed so far.

The precision of the orbit model has continually improved, as indicated by the rms error per degree of freedom in the graph in Fig. 15. Here we see that the rms error has steadily decreased with each major improvement to the model. However, we still have significant improvements to make before we reach the limit of the precision ($\sim$0.015 s) with which we can determine the midtime of a ring occultation profile in the presence of random noise in the data. Some of the effects that might be causing the large residuals are: (i) systematic errors in the times reported at different observing stations for the same occultation; (ii) velocity errors in the ephemeris of Uranus; (iii) the manner in which the midtimes are defined for the rings of irregular structure such as the α Ring; and (iv) unknown causes.

Other effects, which have been discussed by Freedman et al. (1983), are (i) the motion of Uranus relative to the barycenter of the system between the immersion and emersion occultations; (ii) the forced ring precession due to possible shepherd satellites between the rings; and (iii) perturbations of the orbits from ellipses, again due to the possible shepherds.

IV. IMAGING AND SPECTRA

While the systematic observation of stellar occultations has led to a detailed picture of the kinematics, widths, optical depths and radial structure of the Uranian rings (as discussed in the preceding sections), our knowledge concerning the nature of the ring particles themselves is much less complete. In particular, we know neither the composition of these particles nor their size distribution. The most direct way of approaching these questions is to study both the spectral and spatial distribution of sunlight reflected from the rings. Knowledge of the reflection spectrum will constrain, and perhaps uniquely specify, the surface composition of the ring particles, while information on the particle size distribution can be obtained from a study of the phase function of the rings at different wavelengths. Information on the particle size distribution can also be obtained from occultation observations at different wavelengths. A fourth potential source of valuable information concerning both composition and particle size is the spectrum of thermal flux emitted from the rings.

Unfortunately, the possibilities for making such observations with Earth-based telescopes are extremely limited for several reasons. Foremost of these is the extreme narrowness of the rings and thus their small projected area on the sky (1.3% of the area of Uranus' disk, under the most favorable conditions). This, combined with a maximum angular diameter of the ring system of only 8 arcsec, makes direct observations virtually impossible except at wavelengths corresponding to deep absorption bands in the spectrum of Uranus. Sufficiently deep bands, due largely to CH_4, occur only in the near infrared (0.8–4.0 μm), precluding useful visual photoelectric or photographic observations of the rings. Two further limitations on Earth-based observations stem from Uranus' great distance from the Sun: a maximum observable phase angle of only 3°.1, and an equilibrium temperature for dark, isothermal ring particles of 65 K. At this temperature, and for a particle geometric albedo of 0.03 (see below), thermal emission from the rings exceeds reflected sunlight only for wavelengths longer than 11.5 μm, where the Earth's atmosphere is largely opaque. In the radio region, the anticipated thermal flux from the rings, $\sim$0.07 mJy at a wavelength of 3 cm, or $\sim$0.4% of the measured flux from Uranus, is almost certainly undetectable. Radar observations of the Uranian rings, such as have been successfully made of Saturn's rings, are rendered impractical by a combination of small target area, great distance, a two-way light-travel time of $\sim$5 hr, and, at present, Uranus' southerly declination (which puts it beyond the range of the Arecibo antenna).

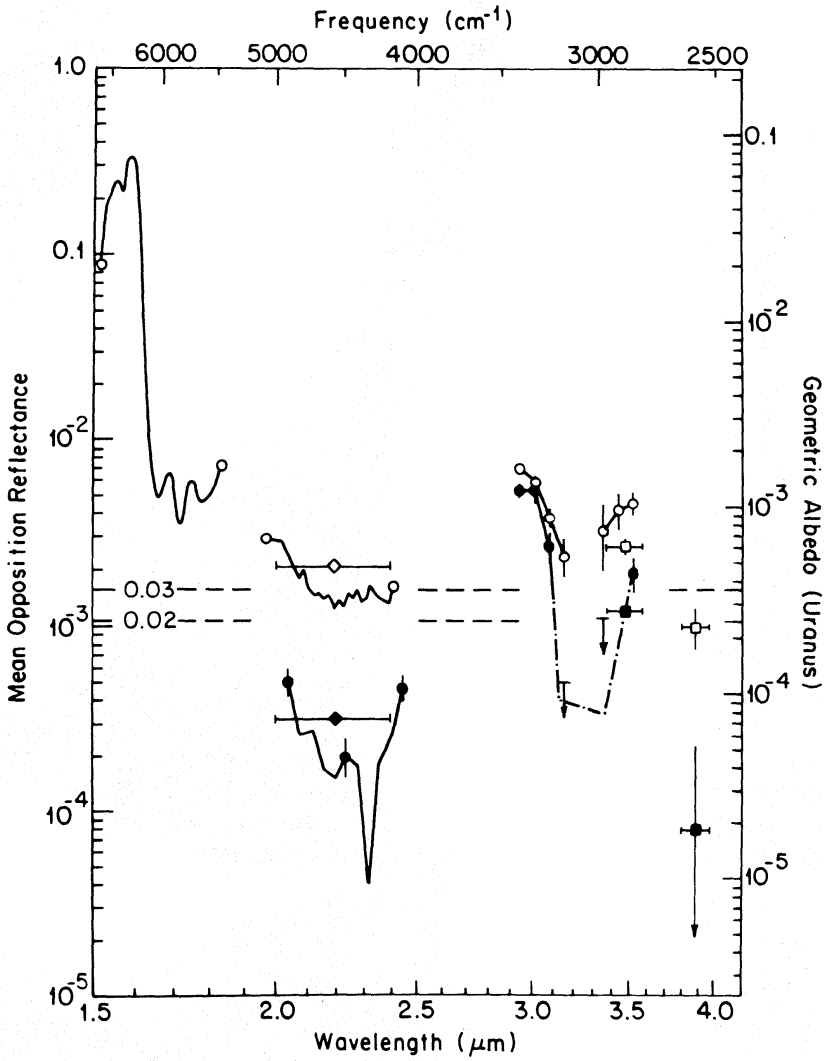

Fig. 16. Spectral reflectances of the Uranian system between 1.5 and 3.9 μm as observed with both large (open symbol) and small (filled symbol) circular apertures centered on Uranus. Solid lines and circles represent circular variable filter data (resolution 0.03 to 0.05 μm); squares represent narrowband filter measurements at 3.48 and 3.89 μm; diamonds represent broadband 2.2 μm measurements. Error bars are included for representative points, when larger than the diameter of the symbols. 1-σ upper limits are shown at 3.15 and 3.36 μm in the small aperture spectrum. Ordinate scale on right gives the geometric albedo of Uranus for an equatorial radius of 25,600 km, and ignores the contribution by the rings to the large aperture data. Horizontal dashed lines indicate the reflectance of the rings alone for ring geometric albedos of 0.02 and 0.03 (figure after Nicholson et al. 1983).

A. Infrared Spectrophotometry

Pending the encounter of Voyager 2 with Uranus in January 1986 and the advent of the Space Telescope, when many of these difficulties should be overcome, we are restricted to observations in selected regions of the near-infrared spectrum. Fig. 16 shows the spectral reflectance of Uranus and its rings in the wavelength range 1.5 to 4.0 μm (Nicholson et al. 1983). It is

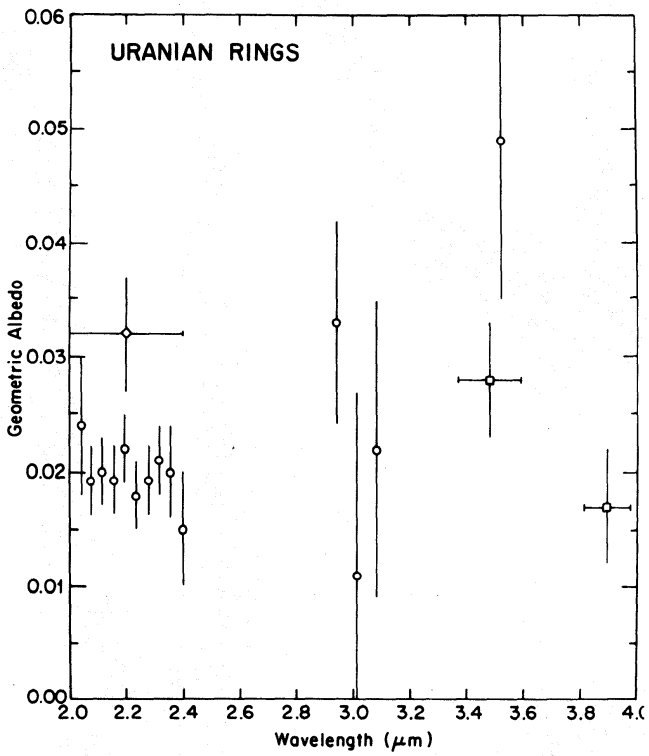

Fig. 17. The geometric albedo of the Uranian rings between 2.0 and 3.9 μm, as derived from the observations and an average integrated ring width of 85 km. Circles, squares, and diamonds have same meaning as in Fig. 16 (figure after Nicholson et al. 1983).

apparent that the rings should be most readily detected and studied in the 2.0–2.5 μm and 3.1–4.0 μm bands. The former is due to a combination of several CH_4 bands and the fundamental pressure-induced vibrational absorption of H_2, while the latter is due to the ν_3 fundamental of CH_4.

Spectrophotometric observations in the 2.0–2.5 μm region, with spectral resolutions of ~0.04 μm, have been published by Nicholson and Jones (1980) and Soifer et al. (1981). These observations have been repeated and extended to the 1.5–1.85 and 2.95–4.0 μm regions by Nicholson et al. (1983), whose derived albedo spectrum for the rings is shown in Fig. 17. This spectrum was obtained by subtracting the spectrum of Uranus, recorded with small circular apertures of 3.5 to 5.9 arcsec diameter, from the combined spectrum of Uranus plus rings recorded with 10 to 12 arcsec diameter apertures. This method can obviously provide reliable results only at wavelengths where the integrated flux from the rings is comparable to, or greater than, that from the planet itself. A significant source of uncertainty in the derived ring albedos lies in the seeing corrections that must be applied to the Uranus spectrum in order to account for planetary flux spilling out of the necessarily undersized small aperture. These corrections are estimated from multi-aperture observations of Uranus at 1.25 and 1.65 μm, where the contributions from the rings are insignificant (Matthews et al. 1982).

Within the uncertainties in the data, the spectrum of the rings appears to be essentially flat between 2.0 and 4.0 μm. Average geometric albedos, calculated for an integrated effective width for the 9 rings of 85 km, are 0.020 $\pm$0.003 between 2.08 and 2.40 μm, 0.024 $\pm$0.006 between 2.94 and 3.08 μm, 0.028 $\pm$ 0.005 at 3.5 μm, and 0.017 $\pm$ 0.005 at 3.9 μm. Broadband 2.0–2.4 μm photometry yields a slightly higher value of 0.032 $\pm$ 0.005 (Matthews et al. 1982). These albedos refer to the rings as a whole, and most particularly to the ϵ Ring, which contributes $\sim$70% of the surface area. The geometric albedos of the ring particles must be slightly higher because of the finite ($\tau \simeq 1$ to 2) optical depth of the rings.

At shorter wavelengths, only rough estimates of, or upper limits on, the ring albedo are available. At 0.89 μm, Thomsen et al. (1978) measured a geometric albedo of 0.02 $\pm$ 0.01, while Sinton (1977) and Smith (1977) set upper limits of 0.05 and 0.01, respectively, for integrated ring widths of 100 km. More recently, B. A. Smith and J. A. Westphal (personal communications) have each succeeded in detecting the rings at 1.0 μm using CCD imaging systems, but no useful albedo estimates are available. Nicholson et al. (1983) estimate an upper limit to the ring geometric albedo of 0.02 at 1.7 μm. It appears, therefore, that the rings are quite dark at all wavelengths at which they have been observed, covering, albeit very incompletely, the range 0.89 to 3.9 μm.

While no direct identification of the surface composition of the ring particles can be made from our present knowledge of the reflection spectrum, certain inferences can be drawn from the lack of prominent spectral features in the 2.0–4.0 μm region. First, the ring particles are not covered by substantial amounts of either H_2O or NH_3 frost. This follows from both the very low 2.0–2.4 μm albedo and the absence of a strong absorption feature at 3.0 μm exhibited by both of these materials (Larson and Fink 1977). In addition, H_2O frost absorbs at 2.0 and $>$2.5 μm quite strongly, while NH_3 frost absorbs at 2.0 and 2.2–2.3 μm (Kieffer and Smythe 1974; Larson and Fink 1977). This conclusion is significant in light of the identification of H_2O frost on the surfaces of four of the Uranian satellites (Cruikshank 1980; Cruikshank and Brown 1981; Soifer et al. 1981).

A second constraint from the spectral data is that the surface material of the ring particles does not contain appreciable quantities of bound or adsorbed H_2O. Hydrous materials invariably show a broad, strong absorption feature centered at 2.9–3.0 μm (Hovis 1965; Fink and Burk 1973; Pollack et al. 1978), which is not apparent in the ring spectrum. This feature persists even when opaque materials such as carbon are mixed with the hydrous material (Larson et al. 1979), although the weaker 1.4 and 1.9 μm H_2O features may be suppressed in such a mixture (Johnson and Fanale 1973).

A comparison of the spectrum, and more especially the albedo, of the Uranian rings with published spectra of other solar system objects does not reveal any likely matches. Among the meteorites, only carbonaceous chond-

rites, ureilites and "black chondrites" have 2.0–2.5 μm reflectances ($\simeq$ Bond albedos) ≤ 0.10 (Gaffey 1976). Of these, only the primitive C1 and C2 carbonaceous chondrites have reflectances ≤ 0.05, and Larson et al. (1979) have shown that these objects exhibit strong 3.0 μm absorptions due to H_2O. Several small satellites, notably Phobos, Deimos and Amalthea, have visual geometric albedos of 0.04 to 0.06 (Veverka 1977; Smith et al. 1979). Amalthea, however, has a considerably higher reflectance in the 2.0–2.5 μm region (Neugebauer et al. 1981). We still lack 3–4 μm observations of these objects. The leading (i.e., dark) side of Iapetus has a geometric albedo of ~ 0.12 in the 2.0–2.5 μm region (Soifer et al. 1979), and a deep absorption feature at 3.0 μm which is evidently due to small amounts of H_2O frost (Lebofsky et al. 1982). A few data are available concerning the infrared spectra (>1.1 μm) of asteroids (Larson and Veeder 1979). C-type asteroids have relatively flat 0.6–2.2 μm spectra and geometric albedos ≤ 0.065, with some as low as 0.02–0.03 (Morrison and Lebofsky 1979). The best-studied asteroid of this type, 1 Ceres, exhibits a pronounced 3.0 μm absorption, interpreted in terms of bound H_2O in the surface material (Lebofsky 1978; Larson et al. 1979; Lebofsky et al. 1981), although not all C-type asteroids show this feature (Lebofsky 1980).

Is it possible that the rings are uniformly dark in backscattered light because the scattering cross section is dominated by particles with sizes comparable to, or smaller than, the wavelengths of observation, rather than because the particles themselves are intrinsically dark? A direct answer to this question should be provided by Voyager 2, which will observe the rings at a wide range of phase angles. At present, the particle size distribution in the rings is constrained by the mean surface densities derived from their observed eccentricity gradients using the Goldreich and Tremaine model (see Table V). For the ϵ Ring, a mean surface density of 26 g cm^{-2}, combined with an estimated mean optical depth of ~ 2, suggests an effective particle diameter of 20 cm, for a particle density of 1 g cm^{-3}. It is difficult, although perhaps not impossible, to construct a size distribution which reconciles this effective, mass-weighted diameter with an effective diameter for light scattering of ~ 1 μm. There also does not appear to be a strong dependence of the geometric albedo of the rings on wavelength, which provides a further argument against scattering by micron-sized particles. Finally, the occultation profiles of the rings have as yet shown no discernable differences for wavelengths of 0.62, 0.75, 0.85 and 2.2 μm, again arguing for a small population of micron-sized particles.

B. 2.2 μm Mapping

With the above-mentioned exception of CCD observations at either 0.89 or 1.0 μm, there are no presently available astronomical techniques capable of directly imaging the Uranian rings from the surface of the Earth. (This situation may, however, soon be remedied by the development of arrays of infrared

detectors.) Because of the greatly reduced scattering of planetary flux, and the absence of atmospheric seeing, the Space Telescope should provide useful visual images after the Voyager 2 encounter. Even the Space Telescope, of course, will not be able to resolve the 10^{-4} to 10^{-2} arcsec widths of the rings, although it should permit studies of the photometric and spectroscopic properties of individual rings (see Chapter by Smith).

It is possible, however, to produce maps of the broad distribution of reflected light from the rings from scans of the system made with an infrared photometer in the 2.2 μm (K) band. Two such maps, with resolutions of 5 arcsec (or 65,000 km), are presented in Fig. 18, and again in Fig. 19 in the form of gray-scale images. These figures have been adapted from Matthews et al. (1982). The maps were actually produced from sets of simultaneous 1.6 and 2.2 μm scans. At 1.6 μm, only the planet appears, while at 2.2 μm the (integrated) brightness of the ring system is about three times that of Uranus. The 1.6 μm scans may, therefore, be used to subtract the planetary component from the 2.2 μm scans, leaving the contribution from the rings alone.

The principal significance of these maps is that they are sensitive to the possible presence of broad, optically thin, components of the ring system, such as have been reported by Bhattacharyya and Bappu (1977). Material with a normal optical depth $\leqslant 0.05$, distributed smoothly, is extremely difficult to detect in stellar occultation recordings, although if spread over the 9000 km radial range of the 9 narrow rings, such material could account for up to 80% of the light reflected by the system. That this situation is, in fact, not the case is demonstrated by the approximately 2:1 azimuthal brightness variation exhibited by both maps. This variation is primarily due to the variable width of the ϵ Ring (see Figs. 8 and 10), which provides $\sim 70\%$ of the total surface area of the narrow rings. The position angle of minimum ring brightness in each map coincides with the predicted position angle of the periapse, or narrowest part, of this ring based on the kinematic model described in Sec. III. In contrast to this observed azimuthal variation, any broad component of the ring system should appear axially symmetric, because of the rapidity with which any clumps of material are sheared out by the orbital motion of the particles (period ~ 8 hr). A quantitative comparison of the ratio of observed brightnesses at the positions of the ϵ Ring apoapse and periapse with the predicted ratio based on computer-generated model maps leads to an upper limit of 0.003 on the optical depth of any *axisymmetric* ring component with a nominal width of 5000 km (Matthews et al. 1982). These model maps, shown also in Figs. 18 and 19, incorporate the known width variation and apsidal precession of the ϵ Ring, as well as a constant integrated width of 30 km for the other 8 rings (the width variations of the α and β Rings are comparatively unimportant, in this context). In addition, the above-mentioned comparison of brightness ratios takes into account a variation in optical depth around the ϵ Ring, in inverse proportion to the width variation. If the ϵ Ring's optical depth is, on the other hand, essentially constant (an unlikely possibility) then

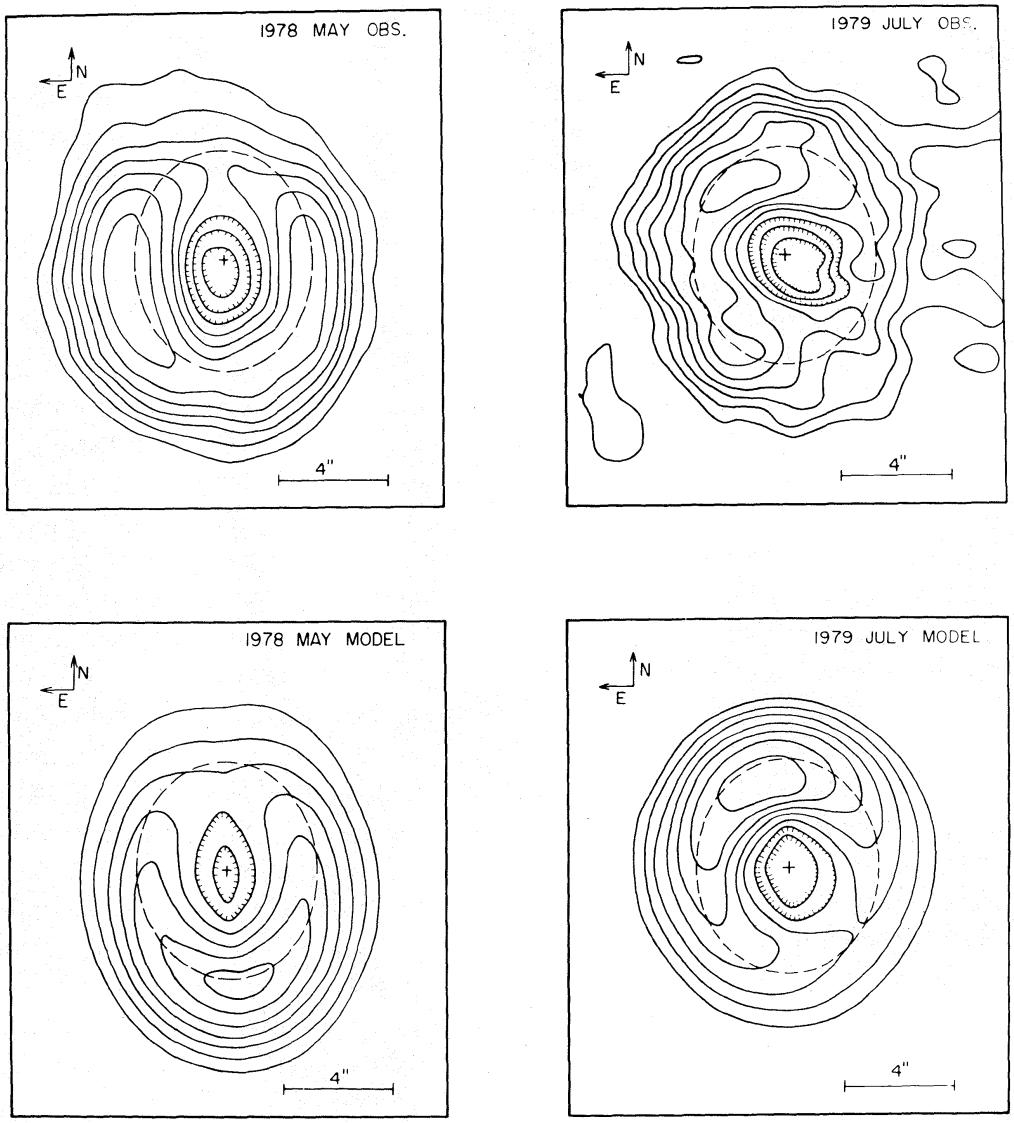

Fig. 18. Contour maps of reflected light from the rings of Uranus at a wavelength of 2.2 μm. Simultaneous observations at 1.5 or 1.65 μm were used to subtract the planetary component of flux at 2.2 μm, as described in the text. Also shown are model maps constructed for the dates on which the observations were made. The model consists of a single circular ring whose brightness is proportional to the projected integrated width of the nine known narrow rings, and whose orientation and precession rate are those determined for the ϵ Ring from occultation observations (see text). The location of the ϵ Ring is indicated by a dashed ellipse, while the cross represents the center of Uranus' disk, which has a diameter of $\sim$4 arcsec. The maps cover an area of 16 $\times$ 16 arcsec. Contours represent flux levels on an arbitrary but linear scale, with the scale of the models adjusted to match that of the observations. Zero and negative contours are suppressed for clarity; the 1-σ noise level in the 1978 map is $\pm$0.4 contour interval, and $\pm$0.6 contour interval in the 1979 map. Resolution of all maps is $\sim$5 arcsec, as determined by the convolution of the 4-arcsec scanning aperture with seeing of 1.5 to 2 arcsec. (a) Map constructed by averaging eight sets of scans made on 19 May 1978; (b) Map constructed by averaging four sets of scans on 6 and 7 July 1979; (c) Model map for 19 May 1978; (d) Model map for 6–7 July 1979 (figure after Matthews et al. 1982).

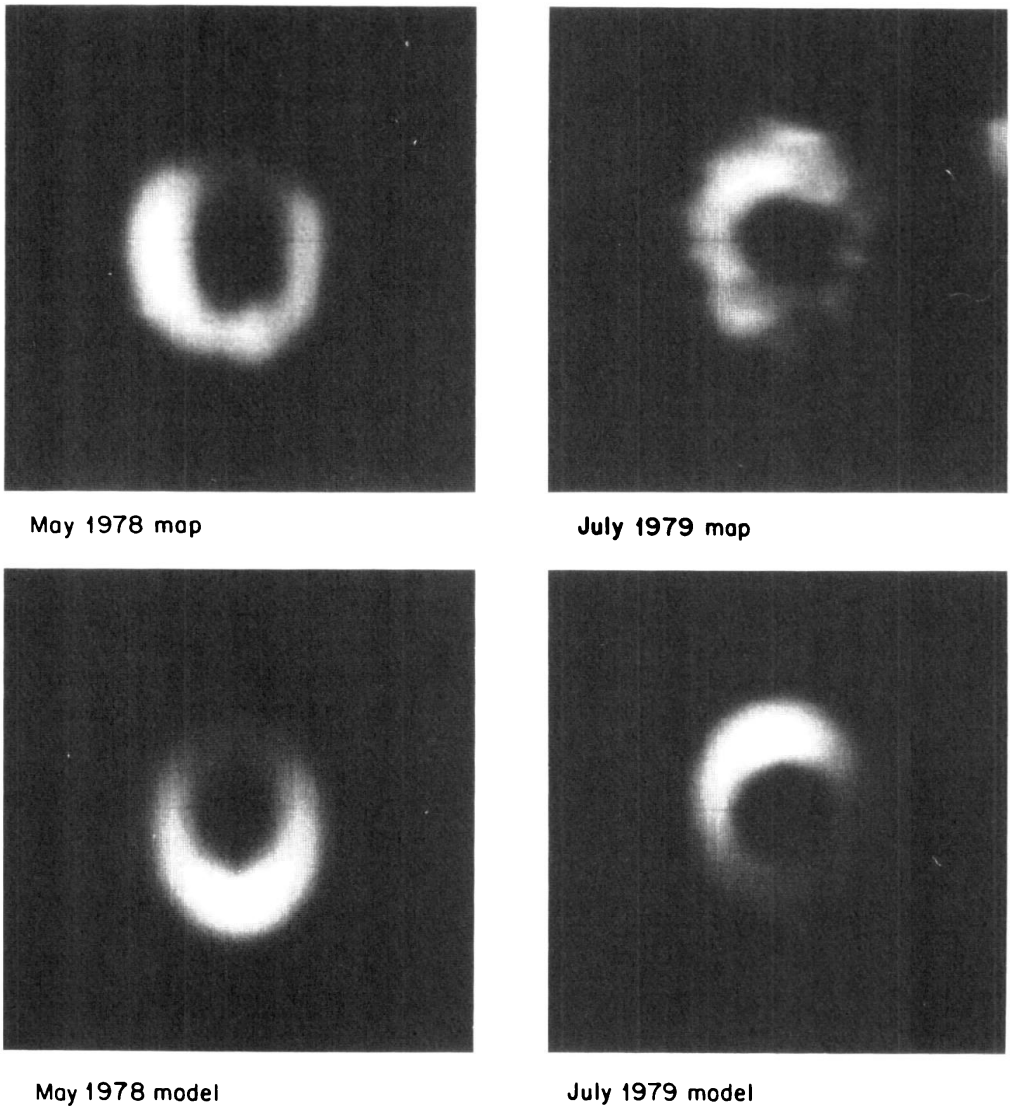

Fig. 19. Gray-scale images of the rings of Uranus, derived from contour maps in Fig. 18. The May 1978 map represents the average of 4 hr of observations on the Hale 5-m telescope on 19 May 1978, and the July 1979 map a total of 2 hr of observation on 6 and 7 July 1979. Resolution of the images is ~5 arcsec, as set by the convolution of the 4 arcsec diameter scanning aperture with atmospheric seeing. Each image covers an area of 20 × 20 arcsec, centered on Uranus. North up, east to the left. Below each observed map is a model map for that date, based on stellar occultation observations and a computer simulation of the scanning procedure used to obtain the real maps. The model incorporates the known width variation and apsidal precession rate of the ϵ Ring, as well as a constant integrated width of 30 km for the other 8 rings. The satellite Ariel ([2.2 μm] = 13.0) appears on the western edge and again, more faintly, on the eastern edge of the 6–7 July 1979 map. Miranda (estimated [2.2 μm] ~15) was too faint and/or fast moving to detect in these data (figure adapted from Matthews et al. 1982).

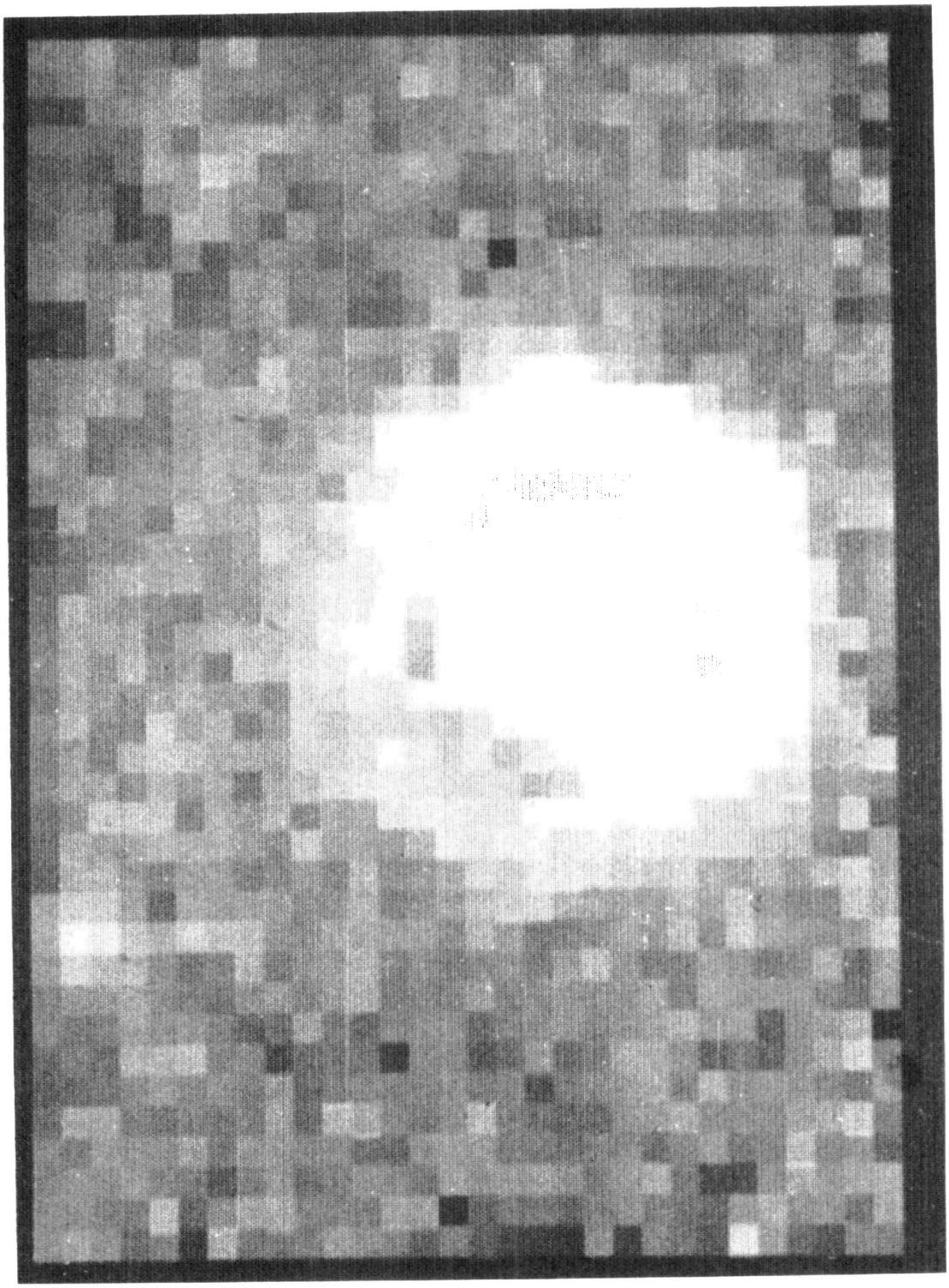

Fig. 20. Image of Uranus and its rings at 2.2 μm, taken in May 1982 by Allen (1983). East is to the left and north is upward on the page. Satellite Miranda appears near the left edge of the picture. (Copyright 1982, Anglo-Australian Telescope Board.) See Color Plate 1 for a more recent color image of the rings of Uranus by D. Allen.

the upper limit is raised to ~0.010. Either limit is considerably below the value of ~0.025 reported by Bhattacharyya et al. (1979), based on low amplitude, low-frequency photometric variations in an occultation recording from 10 March 1977. Implicit in the above discussion is the assumption that the 2.2 μm albedo of the particles in any extended, optically thin ring is equal to, or greater than, that of the particles in the narrow rings.

Although the principal features of the 2.2 μm maps may be understood in terms of the known widths and kinematics of the rings, the significant enhancement in brightness of the east side of the system relative to the west side observed in May 1978 is not. It has been shown (Matthews et al. 1982) that the effect cannot be explained in terms of a bright satellite or condensation within the rings, a background star, or differences between the brightness distributions across the disk of Uranus at 1.6 and 2.2 μm. Again, a broad, axisymmetric ring should not produce such an asymmetry in the brightness distribution. In May 1982, when the periapse of the ϵ Ring was located in the south rather than in the north as in May 1978, Allen (1983) obtained a third 2.2 μm map of the rings (Fig. 20) which shows an enhancement in brightness of the west side. This suggests that the anomalously bright region precesses with the apsidal line of the ϵ Ring, although this tentative conclusion should be tested by further observations. The location of the bright region in the quadrant following passage of the ring particles through periapse, where collisions are most probable (Dermott and Murray 1980), suggests further that the phenomenon may be due to scattering from collisional debris, which is subsequently reaccreted. However, no evidence of such debris has been found in occultation profiles of the ϵ Ring.

V. THE RINGS AS PROBES OF URANUS

Studies of the Uranian rings, and in particular the development of precise kinematic models for the ring orbits, have led to a considerable improvement in our knowledge of several important parameters of Uranus itself. First is the determination of the gravity harmonic coefficients J_2 and J_4 from the apsidal and nodal precession rates of the eccentric and/or inclined rings (see Table VI). The control on J_4, whose influence on precession rates drops off as $a^{-11/2}$, stems from the close proximity of the rings to the planet. From Table VII, which compares the gravity coefficients of Uranus with those of Jupiter and Saturn, obtained from spacecraft flybys, we see that the Voyager flyby of Uranus in 1986 is unlikely to improve on the precision obtainable from the ring orbits. Improved accuracy, however, should come from a more accurate determination of GM_u, which is a source of systematic error in J_2 that could well be greater than its current uncertainty (see Table VI).

Secondly, the rings serve as a precise reference system for locating occultation-derived atmospheric temperature and density profiles with respect to the center of mass of Uranus. This has permitted a determination of the

TABLE VII

Rotation Periods of the Jovian Planets[a]

	Jupiter	Saturn	Uranus	Neptune
Oblateness (ϵ)	0.0648 ± 0.0001[1]	0.088 ± 0.006[4]	0.024 ± 0.003[7]	0.021 ± 0.004[12]
Equatorial radius (R_ϵ, km)	$71{,}541 \pm 4$[1]	$60{,}000 \pm 500$[4]	$26{,}145 \pm 30$[7]	$25{,}225 \pm 30$[12]
$GM \times 10^{-3}$ ($km^3\ s^{-2}$)	$126{,}686.9 \pm 0.5$[2]	$37{,}939 \pm 2$[5]	$5{,}784 \pm 4$[9]	$6{,}787 \pm 5$[13]
$J_2 \times 10^3$	14.733 ± 0.004[2]	16.479 ± 0.018[5]	3.349 ± 0.005[8]	3.5 ± 0.4[14]
$J_4 \times 10^6$	-587 ± 7[2]	-937 ± 38[5]	-38 ± 9[8]	?
Reference radius (R_r, km)	71,398	60,000	26,200	25,225
Calculated rotation period (Eq. [9] in text)	$9^h\ 54^m\ 52^s \pm 44^s$	$11^h\ 19^m \pm 37^m$	15.6 ± 1.4 hr	14.9 ± 1.6 hr
Measured rotation period	$9^h\ 55^m\ 29^s.71 \pm 0^s.04$[3]	$10^h\ 39^m\ 24^s \pm 7^s$[6]	16.2 ± 0.3 hr[10] (24 ± 3 hr[11])	17.7 ± 0.1 hr[15]
Difference (measured–calculated)	$38^s \pm 44^s$	$40^m \pm 37^m$	0.6 ± 1.4 hr	2.8 ± 1.6 hr

[a]Errors have been estimated when not explicitly given by the original source, and the error in the calculated period reflects that introduced by the error in the oblateness.

[b]References: 1. Lindal et al. (1981); 2. Null (1976); 3. Smoluchowski (1976); 4. Gehrels et al. (1980); 5. Null et al. (1981); 6. Desch and Kaiser (1981); 7. Elliot et al. (1981*a*); 8. Table VI in text; 9. Dunham (1971); 10. Goody (1982); 11. Hayes and Belton (1977); 12. Kovalesky and Link (1969); 13. Gill and Gault (1968); 14. Harris, personal communication, 1982; 15. Brown et al. (1981).

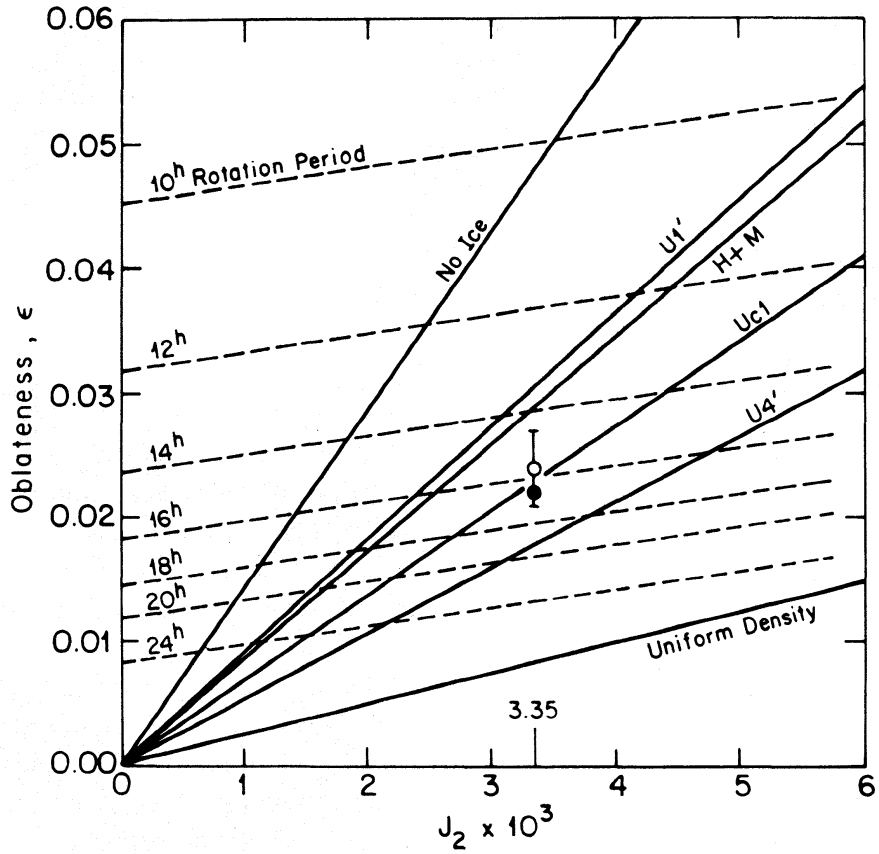

Fig. 21. Predicted values of oblateness, ϵ, and J_2 as a function of rotation period of several recently published interior models of Uranus. The open symbol represents the current best estimates of these two quantities based on stellar occultation observations of both planet and rings (see text and Table VI), while the filled symbol indicates Franklin et al.'s (1980) determination of $\epsilon = 0.022 \pm 0.001$, based on stratoscope images. Models U1′ (Podolak and Reynolds 1981) and H + M (Hubbard and MacFarlane 1980) are essentially equivalent and consist of three compositionally distinct layers (a rocky core of mass $\sim 3\ M_\oplus$, an "ice" layer of $\sim 10\ M_\oplus$, and a solar-composition envelope of $\sim 1.5\ M_\oplus$) while models Uc1 and U4′ (Podolak and Reynolds 1981) incorporate various degrees of enrichment of H_2O, NH_3 and CH_4 in the outer envelope. Also shown are extreme models, corresponding to (i) a uniform density planet, and (ii) a rocky core surrounded by a pure H_2-He envelope ("no ice"). Figure is adapted from Hubbard and MacFarlane (1980) and Podolak and Reynolds (1981).

planet's oblateness (ellipticity) ϵ which is independent of the recent redetermination of the optical oblateness by Franklin et al. (1980). The measured oblateness, at a molecular number density level of $\sim 8 \times 10^{13}$ cm^{-3}, is 0.024 ± 0.003 (Elliot et al. 1981*a*), in good agreement with Franklin et al.'s 0.022 ± 0.001. The corresponding equatorial radius at this same level is $26{,}145 \pm 30$ km, corresponding to a cloud-top radius of $\sim 25{,}600 \pm 100$ km.

From a knowledge of both J_2 and ϵ, and the assumption of hydrostatic equilibrium, a third important parameter may be calculated, namely the rotation period of the planet. Uranus' rotation period has proved extremely resis-

tant to determination by the usual photometric and spectroscopic techniques, which have produced ambiguous and/or discordant results (Goody 1982). The rotation period P is given by the relation (Brouwer and Clemence 1961):

$$P = 2\pi \left[\frac{R_e^3(1-\epsilon)\,(1+\frac{3}{2}J_2)}{2GM\,(\epsilon-\frac{3}{2}J_2 - \frac{5}{8}J_4 - \frac{9}{4}J_2^2)} \right]^{\frac{1}{2}} . \tag{9}$$

The quantity R_e refers to the equatorial radius for which the geometric oblateness is ϵ.* If the reference radius R_r for the harmonic expansion of the gravity potential does not equal R_e, then defining $\rho = R_r/R_e$ one must substitute $\rho^2 J_2$ for J_2 and $\rho^4 J_4$ for J_4 in Eq. (9).

From the occultation-derived values for J_2, J_4 and ϵ, a rotation period of $P = 15.6 \pm 1.4$ hr is obtained. If Franklin et al.'s value of ϵ is used, the result is $P = 16.6 \pm 0.5$ hr. Although the assumption of hydrostatic equilibrium may be questionable, the basic soundness of this procedure is shown by the comparison in Table VII of the periods derived for Jupiter and Saturn from their measured values of J_2, J_4 and ϵ with the directly determined (radio) periods.

Accurate values of J_2, J_4, ϵ and P are of great importance in constraining interior models of Uranus. In Fig. 21 the predicted values of J_2 and ϵ, as a function of rotation period, for several recently constructed interior models (Hubbard and MacFarlane 1980; Podolak and Reynolds 1981) are compared with the measured values of these quantities. Already the constraint is useful, although a more accurate determination of P, independent of ϵ, is clearly necessary.

The fourth parameter that has now been determined with improved precision from studies of the rings is the orientation of Uranus' rotation axis (see Table VI). This was previously obtained from astrometric studies of the orbits of Uranus' five satellites (Dunham 1971), but use of the ring-determined pole direction in a reanalysis of the satellite observations might lead to improvements in the other orbit parameters.

Finally, analysis of stellar occultations by the rings is resulting in an accumulation of data that can eventually be used to improve our knowledge of the orbit of Uranus in relation to the celestial coordinate system. The position of each occulted star, relative to the orbit of Uranus, is known to a precision of $\sim 0''.01$ (see e.g., Elliot et al. 1981*a*).

VI. FUTURE OBSERVATIONS

We can expect to learn a great deal more about the rings of Uranus during the next few years through groundbased observations, the Space Telescope and the Voyager encounter during January 1986. From groundbased observations, we can improve the kinematic model for the orbits. The improved

*Geometric oblateness is defined by $\epsilon = 1 - R_p/R_e$, where R_e and R_p are equatorial and polar radii.

model may allow the detection of effects due to unseen satellites within the rings. These satellites would cause the shapes of the rings to deviate from ellipses and also cause them to precess faster than presently modeled (Freedman et al. 1983). Also, we should make significant progress in our understanding of the ring profiles. If a bright enough star is occulted, perhaps we can detect inter-ring material.

With the planetary camera on the Space Telescope, we hope to separate nearly all nine rings and determine their individual albedos. For occultation observations with the high-speed photometer, scintillation noise will be absent, which will allow a more extensive search for inter-ring material. Also, occultations observed in the far ultraviolet will have better spatial resolution than current 2μm data by a factor of three, because of the smaller Fresnel scale.

The Voyager encounter will provide much more information about the rings, particularly from the occultation, tracking and imaging data. According to A. L. Lane (personal communication), several stellar occultations will be visible. These should provide spatial resolution up to 100 times better than achievable from Earth-based occultations, which would revolutionize our knowledge of the ring structure. Two occultations of radio signals transmitted by the spacecraft will also occur (Stone 1982) providing information on the abundance of cm- and larger-sized ring particles.

The resolution of the imaging will not be as good as we have already achieved with groundbased occultations, but would provide phase functions of the rings at different wavelengths, hopefully shedding further light on particle size distribution. The imaging data should also provide a more sensitive search for inter-ring material and the postulated confining satellites (Goldreich and Tremaine 1979*a*). It is possible that an analysis of images of the rings with different viewing geometries could lead to a refinement in the orientation of Uranus' rotation axis, which would in turn lead to reduction of the current ± 17 km uncertainties in the absolute semimajor axes of the rings.

The tracking data will yield values for GM_u and J_2. Although the Voyager value for J_2 will not be as precise as that already obtained from the occultation data (Stone 1982), it should prove useful as an independent check on the latter. Infrared observations would certainly be of interest, but the low temperature and small area of the rings may prevent their detection by the Voyager infrared radiation spectrometer (IRIS).

VII. DISCUSSION

Apparently the Uranian system has an intermediate amount of material in comparison with the low optical-depth Jovian ring and the impressive ring system that surrounds Saturn. Since the Saturnian system contains relatively few free gaps, much of the theory describing the Saturnian system deals with wave phenomena in a continuous distribution of particles. For Uranus, we

have nine discrete rings, and the theoretical problems are mainly concerned with explaining the dynamics of narrow rings and their sharp edges.

Two types of mechanism of ring confinement, both involving unseen satellites, have been proposed and investigated (see chapter by Dermott). For the "shepherd" satellite mechanism of Goldreich and Tremaine (1979*a*), each of the narrow rings would have a pair of satellites keeping it from spreading. The inclinations and eccentricities of the rings would then be forced by the satellites, which would be in eccentric and inclined orbits (Goldreich and Tremaine 1981). The model of Dermott et al. (1979) invokes satellites within the rings, whose particles move on horseshoe orbits. A recent explanation for sharp edges in terms of satellite resonances (Borderies et al. 1982) has not yet been applied to the Uranian rings. In the shepherd picture, the uniform precession of the rings is explained by the self-gravity of the ring (Goldreich and Tremaine 1979*b*; Borderies et al. 1983), an explanation not universally accepted (Dermott and Murray 1980). An important potential achievement of the Voyager flyby would be the detection of, or placing a significant upper limit on, the presence of these postulated satellites.

Further observational constraints on the confinement mechanism would be placed through the detection of inter-ring material. Such material must exist, at some level, since the smallest particles would leak out of a narrow ring due to the Poynting-Robertson effect (see chapter by Mignard) or plasma drag (see chapter by Grün et al.), if Uranus possesses a significant magnetic field.

Other theoretical work is needed to produce models that explain the details of the ring structure for the α, η and ϵ Rings. Important information for this work would be the particle size distribution and velocity dispersion, which are not presently known.

Once the present dynamics of the rings are well understood, we can then extrapolate these processes back in time, with the hope of inferring the age and possibly the origin of the rings. In this context, another question that must be answered is why the surfaces of the ring particles are not icy, as are the surfaces of the Uranian satellites (Cruikshank and Brown 1981) and the particles in Saturn's rings.

For the next few years, at least, we expect significant progress towards answering these questions, both from comparative studies with Saturn's narrow ringlets and from new observations of the Uranian rings from the ground, the Space Telescope, and the Voyager 2 encounter in 1986.

Acknowledgments. We are grateful to referees S. Dermott and B. Sicardy for their constructive criticisms of this review. Helpful comments and information were also provided by D. Allen, L. Esposito, R. French, R. Greenberg, A. Harris, K. Matthews, K. Meech and S. Tremaine. Uranian ring research has been supported, in part, by grants from NASA and NSF.

REFERENCES

Allen, D. A. 1983. Infrared views of the giant planets. *Sky Telescope* 65:110–112.

Bhattacharyya, J. C., and Bappu, M. K. V. 1977. Saturn-like ring system around Uranus. *Nature* 270:503–506.

Bhattacharyya, J. C., and Kuppuswamy, K. 1977. A new satellite of Uranus. *Nature* 267:331–332.

Bhattacharyya, J. C., Bappu, M. K. V., Mohin, S., Mahra, H. S., and Gupta, S. K. 1979. Extended ring system of Uranus. *Moon Planets* 21:393–404.

Borderies, N., Goldreich, P., and Tremaine, S. 1982. Sharp edges of planetary rings. *Nature* 299:209–211.

Borderies, N., Goldreich, P., and Tremaine, S. 1983. Precession of inclined rings. *Astron. J.* 88:226–228.

Bouchet, P., Perrier, C., and Sicardy, B. 1980. Occultation by Uranus. *I.A.U. Circ.* No. 3503.

Brahic, A. 1982. Planetary rings. In *Formation of Planetary Systems*, ed. A. Brahic (Toulouse: Cepadues Editions), pp. 651–724.

Brouwer, D. 1946. The motion of a particle of negligible mass under the gravitational attraction of a spheroid. *Astron. J.* 51:223–231.

Brouwer, D. 1959. Solution to the problem of artificial satellite theory without drag. *Astron. J.* 64:378–397.

Brouwer, D., and Clemence, G. M. 1961. Orbits and masses of planets and satellites. In *The Solar System III*, eds. G. P. Kuiper and B. M. Middlehurst (Chicago: Univ. of Chicago Press), pp. 31–94.

Brown, R. H., Cruikshank, D. P., and Tokunaga, A. T. 1981. The rotation period of Neptune's upper atmosphere. *Icarus* 47:159–165.

Chen, D.-H., Yang, H.-Y., Wu, C.-H., Wu, Y.-C., Kiang, S.-Y., Huang, Y.-W., Yeh, C.-T., Chai, T.-S., Hsieh, C.-C., Cheng, C.-S., and Chang, C. 1978. Photoelectric observation of the occultation of SAO 158687 by Uranian ring and the detection of Uranian ring signals from the light curve. *Scientia Sinica* XXI:503–508.

Churms, J. 1977. Occultation of SAO 158687 by Uranian satellite belt. *I.A.U Circ.* No. 3051.

Cruikshank, D. P. 1980. Near-infrared studies of the satellites of Saturn and Uranus. *Icarus* 41:246–258.

Cruikshank, D. P., and Brown, R. H. 1981. The Uranian satellites: Water ice on Ariel and Umbriel. *Icarus* 45:607–611.

Dermott, S. F., and Murray, C. D. 1980. Origin of the eccentricity gradient and apse alignment of the ϵ ring of Uranus. *Icarus* 43:338–349.

Dermott, S. F., Gold, T. G., and Sinclair, A. T. 1979. The rings of Uranus: Nature and origin. *Astron. J.* 84:1225–1234.

Desch, M. D., and Kaiser, M. L. 1981. Voyager measurement of the rotation period of Saturn's magnetic field. *Geophys. Res. Letters* 8:253–256.

Dunham, D. W. 1971. Motions of the Satellites of Uranus. Ph.D. dissertation, Yale Univ.

Elliot, J. L. 1977. Signal-to-noise ratios for occultations by the rings of Uranus, 1977–1980. *Astron. J.* 82:1036–1038.

Elliot, J. L. 1979. Stellar occultation studies of the solar system. *Ann. Rev. Astron. Astrophys.* 17:445–475.

Elliot, J. L. 1982. Rings of Uranus: A review of occultation results. In *Uranus and the Outer Planets*, ed. G. A. Hunt (Cambridge: Cambridge Univ. Press), pp. 237–256.

Elliot, J. L., Dunham, E. W., and Millis, R. L. 1977*a*. Discovering the rings of Uranus. *Sky Telescope* 53:412–416, 430.

Elliot, J. L., Dunham, E. W., and Mink, D. J. 1977*b*. The rings of Uranus. *Nature* 267:328–330.

Elliot, J. L., Dunham, E. W., Wasserman, L. H., Millis, R. L., and Churms, J. 1978. The radii of Uranian rings α, β, γ, δ, ϵ, η, 4, 5 and 6 from their occultation of SAO 158687. *Astron. J.* 83:980–992.

Elliot, J. L., Elias, J. H., French, R. G., Frogel, J. A., Liller, W., Matthews, K., Meech, K. J., Mink, D. J., Nicholson, P. D., and Sicardy, B. 1983. A comparison of Uranian ring occultation profiles from three observatories. *Icarus*. In press.

Elliot, J. L., French, R. G., Frogel, J. A., Elias, J. H., Mink, D. J., and Liller, W. 1981*a*. Orbits of nine Uranian rings. *Astron. J.* 86:444–455.

Elliot, J. L., Frogel, J. A., Elias, J. H., Glass, I. S., French, R. G., Mink, D. J., and Liller, W. 1981*b*. The 20 March 1980 occultation by the Uranian rings. *Astron J.* 86:127–134.

Elliot, J. L., Veverka, J., and Millis, R. L. 1977*c*. Uranus occults SAO 158687. *Nature* 265:609–611.

Esposito, L. W., Borderies, N., Goldreich, P., Cuzzi, J. N., Holberg, J. B., Lane, A. L., Pomphrey, R. B., Terrile, R. J., Lissauer, J. J., Marouf, E. A., and Tyler, G. L. 1983. The eccentric ringlet in the Huygens gap at 1.45 Saturn radii: Multi-instrument Voyager observations. *Science*. Submitted.

Fink, U., and Burk, S. D. 1973. Reflection spectra, 2.5–7μ, of some solids of planetary interest. *Comm. Lunar Planetary Lab.* 10:8–20.

Fink, U., and Larson, H. P. 1979. The infrared spectra of Uranus, Neptune and Titan from 0.8 to 2.5 microns. *Astrophys. J.* 233:1021–1040.

Franklin, F. A., Avis, C. C., Colombo, G., and Shapiro, I. I. 1980. The geometric oblateness of Uranus. *Astrophys. J.* 236:1031–1034.

Freedman, A., Tremaine, S. D., and Elliot, J. L. 1983. Weak dynamical forcing of the Uranian ring system. *Astron. J.* 88:1053–1059.

French, R. G., Elliot, J. L., and Allen, D. A. 1982. Inclinations of the Uranian rings. *Nature* 298:827–829.

Gaffey, M. J. 1976. Spectral reflectance characteristics of the meteorite classes. *J. Geophys. Res.* 81:905–920.

Gehrels, T., Baker, L. R., Beshore, E., Blenman, C., Burke, J. J., Castillo, N. D., DaCosta, B., Degewij, J., Doose, L. R., Fountain, J. W., Gotobed, J., KenKnight, C. E., Kingston, R., McLaughlin, G., McMillan, R., Murphy, R., Smith, P. H., Stoll, C. P., Strickland, R. N., Tomasko, M. G., Wijesinghe, M. P., Coffeen, D. L., and Esposito, L. 1980. Imaging photopolarimeter on Pioneer Saturn. *Science* 207:434–439.

Gill, J. R., and Gault, B. L. 1968. A new determination of the orbit of Triton, pole of Neptune's equator, and mass of Neptune. *Astron. J.* 73:S95 (abstract).

Goldreich, P., and Tremaine, S. 1979*a*. Towards a theory for the Uranian rings. *Nature* 277:97–99.

Goldreich, P., and Tremaine, S. 1979*b*. Precession of the ϵ ring of Uranus. *Astron. J.* 84:1638–1641.

Goldreich, P., and Tremaine, S. 1981. The origin of the eccentricities of the rings of Uranus. *Astrophys. J.* 243:1062–1075.

Goldreich, P., and Tremaine, S. 1982. The dynamics of planetary rings. *Ann. Rev. Astron. Astrophys.* 20:249–283.

Goody, R. M. 1982. The rotation of Uranus. In *Uranus and the Outer Planets*, ed. G. A. Hunt (Cambridge: Cambridge Univ. Press), pp. 143–153.

Greenberg, R. 1981. Apsidal precession of orbits about an oblate planet. *Astron. J.* 86:912–914.

Hayes, S. A., and Belton, M. J. S. 1977. The rotational periods of Uranus and Neptune. *Icarus* 32:383–401.

Hovis, W. A. 1965. Infrared reflectivity of iron oxide minerals. *Icarus* 4:425–430.

Hubbard, W. B., and MacFarlane, J. J. 1980. Structure and evolution of Uranus and Neptune. *J. Geophys. Res.* 85:225–234.

Hubbard, W. B., and Zellner, B. H. 1980. Results from the 10 March 1977 occultation by the Uranian system. *Astron. J.* 85:1663–1669.

Johnson, T. V., and Fanale, F. P. 1973. Optical properties of carbonaceous chondrites and their relationship to asteriods. *J. Geophys. Res.* 78:8507–8518.

Kieffer, H. H., and Smythe, W. D. 1974. Frost spectra: Comparison with Jupiter's satellites. *Icarus* 21:506–512.

Klemola, A. R., and Marsden, B. G. 1977. Predicted occultations by the rings of Uranus: 1977–1980. *Astron. J.* 82:849–851.

Klemola, A. R., Mink, D. J., and Elliot, J. L. 1981. Predicted occultations by Uranus: 1981–1984. *Astron. J.* 86:138–140.

Kovalesvsky, J., and Link, F. 1969. Diamètre, aplatissement et propriétés optiques de la haute

atmosphère de Neptune d'après l'occultation de l'étoile BD −17° 4388. *Astron. Astrophys.* 2:398–412.

Kozai, Y. 1959. The motion of a close earth satellite. *Astron. J.* 64:367–377.

Lane, A. L., Hord, C. W., West, R. A., Esposito, L. W., Coffeen, D. L., Sato, M., Simmons, K., Pomphrey, R. B., and Morris, R. B. 1982. Photopolarimetry from Voyager 2: Preliminary results on Saturn, Titan and the rings. *Science* 215:537–543.

Larson, H. P., Feierberg, M. A., Fink, U., and Smith, H. A. 1979. Remote spectroscopic identification of carbonaceous chondrite mineralologies: Applications to Ceres and Pallas. *Icarus* 39:257–271.

Larson, H. P., and Fink, U. 1977. The application of Fourier transform spectroscopy to the remote identification of solids in the solar system. *Appl. Spectrosc.* 31:386–402.

Larson, H. P., and Veeder, G. J. 1979. Infrared spectral reflectances of asteroid surfaces. In *Asteroids*, ed. T. Gehrels (Tucson: Univ. of Arizona Press), pp. 724–744.

Lebofsky, L. A. 1978. Asteroid 1 Ceres: Evidence for water of hydration. *Mon. Not. Roy. Astron. Soc.* 182:17–21.

Lebofsky, L. A. 1980. Infrared reflectance spectra of asteroids: A search for water of hydration. *Astron. J.* 85:573–585.

Lebofsky, L. A., Feierberg, M. A., Tokunaga, A. T., Larson, H. P., and Johnson, J. R. 1981. The 1.7–4.2 μm spectrum of asteroid 1 Ceres: Evidence for structural water in clay minerals. *Icarus* 48:453–459.

Lebofsky, L. A., Feierberg, M. A., and Tokunaga, A. T. 1982. Infrared observations of the dark side of Iapetus. *Icarus* 49:382–386.

Lindal, G. F., Wood, G. E., Levy, G. S., Anderson, J. D., Sweetham, D. N., Hotz, H. B., Bucklesa, B. J., Holmes, D. P., Doms, P. E., Eshleman, V. R., Tyler, G. L., and Croft, T. A. 1981. The atmosphere of Jupiter: An analysis of the Voyager radio occultation measurements. *J. Geophys. Res.* 86:8721–8727.

Liller, W. 1977. Colors and magnitudes of stars occulted by the rings of Uranus, 1977–1980. *Astron. J.* 82:929.

Mahra, H. S., and Gupta, S. K. 1977. Occultation of SAO 158687 by the Uranian rings. *I.A.U. Circ.* No. 3061.

Matthews, K., Neugebauer, G., and Nicholson, P. D. 1982. Maps of the rings of Uranus at a wavelength of 2.2 microns. *Icarus* 52:126–135.

Millis, R. L., and Wasserman, L. H. 1978. The occultation of BD-15° 3969 by the rings of Uranus. *Astron. J.* 83:993–998.

Millis, R. L., Wasserman, L. H., and Birch, P. 1977*a*. Detection of rings around Uranus. *Nature* 267:330–331.

Millis, R. L., Wasserman, L. H., Elliot, J. L., and Dunham, E. W. 1977*b*. The rings of Uranus: Their widths and optical thicknesses. *Bull. Amer. Astron. Soc.* 9:498 (abstract).

Morrison, D., and Lebofsky, L. A. 1979. Radiometry of asteroids. In *Asteroids*, ed. T. Gehrels (Tucson: Univ. of Arizona Press), pp. 184–205.

Neugebauer, G., Becklin, E.E., Jewitt, D. C., Terrile, R. J., and Danielson, G. E. 1981. Spectra of the Jovian ring and Amalthea. *Astron. J.* 86:607–610.

Nicholson, P. D., and Jones, T. J. 1980. Two-micron spectrophotometry of Uranus and its rings. *Icarus* 42:54–67.

Nicholson, P. D., Jones, T. J., and Gatley, I. 1983. The geometric albedo spectra of Uranus and its ring system, 1.5–4.0 μm. In preparation.

Nicholson, P. D., Matthews, K., and Goldreich, P. 1981. The Uranus occultation of 10 June 1979. I. The rings. *Astron. J.* 86:596–606.

Nicholson, P. D., Matthews, K., and Goldreich, P. 1982. Radial widths, optical depths and eccentricities of the Uranian rings. *Astron. J.* 87:433–447.

Nicholson, P. D., Persson, S. E., Matthews, K., Goldreich, P., and Neugebauer, G. 1978. The rings of Uranus: Results of the 10 April 1978 occultation. *Astron. J.* 83:1240–1248.

Null, G. W. 1976. Gravity field of Jupiter and its satellites from Pioneer 10 and Pioneer 11 tracking data. *Astron. J.* 81:1153–1161.

Null, G. W., Lau, E. L., Biller, E. D., and Anderson, J. D. 1981. Saturn gravity results obtained from Saturn Pioneer 11 tracking data and Earth-based Saturn satellite data. *Astron. J.* 86:456–468.

Podolak, M., and Reynolds, R. T. 1981. On the structure and composition of Uranus and Neptune. *Icarus* 46:40–50.

Pollack, J. B., Witteborn, F. C., Erickson, E. F., Strecker, D. W., Baldwin, B. J., and Bunch, T. E. 1978. Near-infrared spectra of the Galilean satellites: Observations and compositional implications. *Icarus* 36:271–303.

Porco, C., Borderies, N., Danielson, G. E., Goldreich, P., Holberg, J. B., Lane, A. L., and Nicholson, P. D. 1983. The eccentric ringlet at 1.29 R_s, In Proceedings of *I.A.U. Colloquium, Planetary Rings*, ed. A. Brahic, Toulouse, France, Aug. 1982.

Ridgway, S. T., Joyce, R. R., White, N. M., and Wing, R. F. 1980. Effective temperatures of late-type stars: The field giants from K0 to M6. *Astrophys. J.* 235:126–137.

Sicardy, B., Combes, M., Brahic, A., Bouchet, P., Perrier, C., and Courtin, R. 1982. The 15 August 1980 occultation by the Uranian system: Structure of the rings and temperature of the upper atmosphere. *Icarus* 52:454–472.

Sinton, W. M. 1977. Uranus: The rings are black. *Science* 198:503–504.

Smart, W. M. 1977. Occultations and eclipses. In *Textbook on Spherical Astronomy* (Cambridge: Cambridge Univ. Press), pp. 368–403.

Smith, B. A. 1977. Uranus rings: An optical search. *Nature* 268:32.

Smith, B. A., Soderblom, L. A., Beebe, R., Boyce, J., Briggs, G., Carr, M., Collins, S. A., Cook, A. F. II, Danielson, G. E., Davies, M. E., Hunt, G. E., Ingersoll, A., Johnson, T. V., Masursky, H., McCauley, J., Morrison, D., Owen, T., Sagan, C., Shoemaker, E. M., Strom, R., Suomi, V. E., and Veverka, J. 1979. The Galilean satellites and Jupiter: Voyager 2 imaging science results. *Science* 206:927–950.

Smoluchowski, R. 1976. Origin and structure of Jupiter and its satellites. In *Jupiter*, ed. T. Gehrels (Tucson: Univ. Arizona Press), pp. 3–21.

Soifer, B. T., Neugebauer, G., and Gatley, I. 1979. The near-infrared reflectivity of the dark and light faces of Iapetus. *Astron. J.* 84:1644–1646.

Soifer, B. T., Neugebauer, G., and Matthews, K. 1981. Near-infrared spectrophotometry of the satellites and rings of Uranus. *Icarus* 45:612–617.

Stone, E. C. 1982. The Voyager encounter with Uranus. In *Uranus and the Outer Planets*, ed. G. Hunt (Cambridge: Cambridge Univ. Press), pp. 275–291.

Taylor, G. E. 1973. An occultation by Uranus. *J. Brit. Astron. Assoc.* 83:352.

Thomsen, B., Baum, W. A., Wilkinson, D. T, and Loh, E. 1978. New results on the albedo of the rings around Uranus. *Bull. Amer. Astron. Soc.* 10:581–582 (abstract).

Veverka, J. 1977. Photometry of satellite surfaces. In *Planetary Satellites*, ed. J. A. Burns (Tucson: Univ. Arizona Press), pp. 171–209.

Yoder, C. F. 1982. The gravitational interaction between inclined, elliptical rings. Preprint.